Earth **Surface**
Dynamics

Landscape response to tectonic deformation and cyclic climate change since ca. 800 ka in the southern central Andes

Elizabeth N. Orr[1,2], **Taylor F. Schildgen**[1,3], **Stefanie Tofelde**[4], **Hella Wittmann**[1], **and Ricardo N. Alonso**[5]

[1]GFZ German Research Centre for Geosciences, Telegrafenberg, 14473 Potsdam, Germany
[2]Department of Geography, Durham University, Durham, DH1 3LE, United Kingdom
[3]Institute for Geosciences, University of Potsdam, Karl-Liebknecht-Str. 24–25, 14476 Potsdam, Germany
[4]Institute of Geological Sciences, Freie Universität Berlin, 12249 Berlin, Germany
[5]Facultad de Ciencias Naturales, Universidad Nacional de Salta, Salta, 4400 Argentina

Correspondence: Elizabeth N. Orr (elizabeth.orr2@durham.ac.uk)

Abstract. Theory suggests that the response time of alluvial channel long profiles to perturbations in climate is related to the magnitude of the forcing and the length of the system. Shorter systems may record a higher frequency of forcing compared to longer systems. Empirical field evidence that system length plays a role in the climate periodicity preserved within the sedimentary record is, however, sparse. The Toro Basin in the Eastern Cordillera of NW Argentina provides an opportunity to test these theoretical relationships, as this single source-to-sink system contains a range of sediment deposits, located at varying distances from the source. A suite of eight alluvial fan deposits is preserved along the western flanks of the Sierra de Pascha. Farther downstream, a flight of cut-and-fill terraces has been linked to eccentricity-driven (100 kyr) climate cycles since ca. 500 ka. We applied cosmogenic radionuclide (^{10}Be) exposure dating to the fan surfaces to explore (1) how channel responses to external perturbations may or may not propagate downstream and (2) the differences in landscape response to forcing frequency as a function of channel length. We identified two generations of fan surfaces: the first (G1) records surface activity and abandonment between ca. 800 and 500 ka, and the second (G2) does so within the last 100 kyr. G1 fans record a prolonged phase of net incision, which has been recognized throughout the central Andes and was likely triggered by enhanced 100 kyr global glacial cycles following the Mid-Pleistocene Transition (MPT). Relative fan surface stability followed, while 100 kyr cut-and-fill cycles occurred downstream, suggesting a disconnect in behavior between the two channel reaches. G2 fans record higher-frequency climate forcing, possibly the result of precessional forcing of climate (ca. 21/40 kyr timescales). The lack of a high-frequency signal farther downstream provides field support for theoretical predictions of a filtering of high-frequency climate forcing with increasing channel length. We show that multiple climate periodicities can be preserved within the sedimentary record of a single basin. Differences in the timing of alluvial fan and fluvial terrace development in the Toro Basin appear to be associated with how channel length affects fluvial response times to climate forcing and local controls on net incision, such as tectonic deformation.

1 Introduction

Fluvial landforms, sediment deposits, and the channel form of alluvial systems can be used to reveal landscape response to past environmental change (Castelltort and Van Den Driessche, 2003, Godard et al., 2013; Dey et al., 2016; Romans et al., 2016; Mescolotti et al., 2021). Alluvial channels respond to climate- or tectonic-driven changes in water discharge, sediment discharge, or base-level elevation by adjusting at least one of their characteristics: bed slope, channel width, channel depth, sediment transport rates, or grain size distribution (Mackin, 1948; Savi et al., 2020). We observe this channel adjustment via sediment aggradation or incision events, which modify channel bed elevations (Howard, 1982; van den Berg et al., 2008; Wickert and Schildgen, 2019; Tofelde et al., 2019). Fluvial landforms such as terraces and alluvial fans, which develop along these channels because of this aggradation or incision, can provide a useful record of how the alluvial channel system has evolved over time (Rohais et al., 2012; Armitage et al., 2013; Kober et al., 2013; Counts et al., 2015; Mather et al., 2017; Tofelde et al., 2021).

Theory suggests that the time required for an alluvial channel long profile to adjust to a change in climate forcing (response time) varies with the magnitude and type of the forcing (sediment supply versus water supply) and the length of the system: shorter systems respond faster and hence may record a higher frequency of forcing compared to longer systems (Paola et al., 1992; Castelltort and Van Den Driessche, 2003; Godard et al., 2013; McNab et al., 2023). The length scale over which periodic forcing delivered at the channel head affects the channel long profile is proportional to the square root of the period of the forcing (Paola et al., 1992), which means that higher-frequency forcing is filtered out with distance downstream. Evidence of this relationship is preserved in several sedimentary basins in the central Andes. Tributary catchments of the Humahuaca Basin ($23°$ S) retain late Quaternary fluvial deposits between 10 and 100 km downstream from the basin headwaters, which record precessional (21 kyr) cycles in aggradation and incision (Schildgen et al., 2016). In the Toro Basin ($24.5°$ S), a flight of fluvial cut-and-fill terraces with periodicity of 100 kyr has been linked to eccentricity-driven climate change (Tofelde et al., 2017). These terraces have an upstream channel length of $\sim$ 60–80 km. Pliocene–Late Pleistocene sediment deposits are preserved $\sim$ 140–160 km downstream from the headwaters of the Iruya Basin ($22°$ S) of the northern central Andes and record long eccentricity (400 kyr) cycles (Fisher et al., 2023). Crucially, only a single climate periodicity has been recorded in each of these basins to date. To further test this theoretical relationship between climate periodicity and system length, we aim to investigate whether multiple periodicities can be preserved within a single basin and, if this is the case, whether higher-frequency climate forcing is only observed in the uppermost reaches of the basin.

Approximately 30 km upstream of the 100 kyr cut-and fill terraces in the Toro Basin is a suite of well-preserved alluvial fan surfaces which extend from tributary catchments that drain the Sierra de Pascha (Fig. 1). There is limited evidence of sediment storage in these tributary catchments en route to the fans. With an upstream channel length of $\sim$ 10 km, this fan record may capture geomorphic change linked to a higher-frequency climate forcing than the downstream terraces. The Toro Basin alluvial channel system therefore allows us to explore (1) how channel responses to external perturbations may or may not propagate downstream and (2) the differences in landscape response to forcing frequency as a function of channel length when comparing the upper-basin alluvial fan deposits with the lower-basin terrace sequence.

To address these aims, we dated the suite of fan surfaces in the upper Toro Basin using in situ [10]Be cosmogenic radionuclide (CRN) dating. We used our new Toro fan chronostratigraphy in conjunction with the fluvial terrace record of Tofelde et al. (2017) to further characterize the evolution of the Toro Basin over the last 1 million years.

2 Regional setting

The Toro Basin ($24.5°$ S) is an intermontane basin in the Eastern Cordillera of NW Argentina, located between the high-elevation Puna Plateau to the west and the low-elevation Andean foreland to the east (Fig. 1). The mainly gravel-bedded Río Toro flows predominantly south from the low-relief upper reaches of the basin with thick successions of preserved sediment, which are the focus of this study (referred to as the upper Toro Basin herein), through a steep bedrock gorge, before draining into the Cabra Corral reservoir in the Lerma Valley (Marrett and Strecker 2000). The diffuse shifts in channel steepness along its course are characteristic of arid, tectonically active landscapes with mechanically strong basement rocks (Fig. 2b and c) (Bernard et al., 2019, Zondervan et al., 2020; Seagren and Schoenbohm, 2021).

2.1 Geology and tectonic setting

The upper Toro Basin is confined by three reverse-fault-bounded basement ranges: (1) the Cumbres de Zamaca bounded by the west-dipping Solá fault in the west, (2) the Sierra de Almagro bounded by the northwest-dipping San Bernardo fault in the north, and (3) the Sierra de Pascha ranges and the east-dipping Gólgota fault in the east (Alonso, 1992; Marrett and Strecker, 2000) (Figs. 1 and 2). The Solá fault has been active since at least the Late Miocene, and tectonic deformation from the Miocene to mid-Pleistocene has been recorded along the San Bernardo and Gólgota faults (Marrett and Strecker, 2000; DeCelles et al., 2011; Pearson et al., 2013; Pingel et al., 2020). The Gólgota fault reactivated after ca. 0.98 Ma (Hilley and Strecker, 2005).
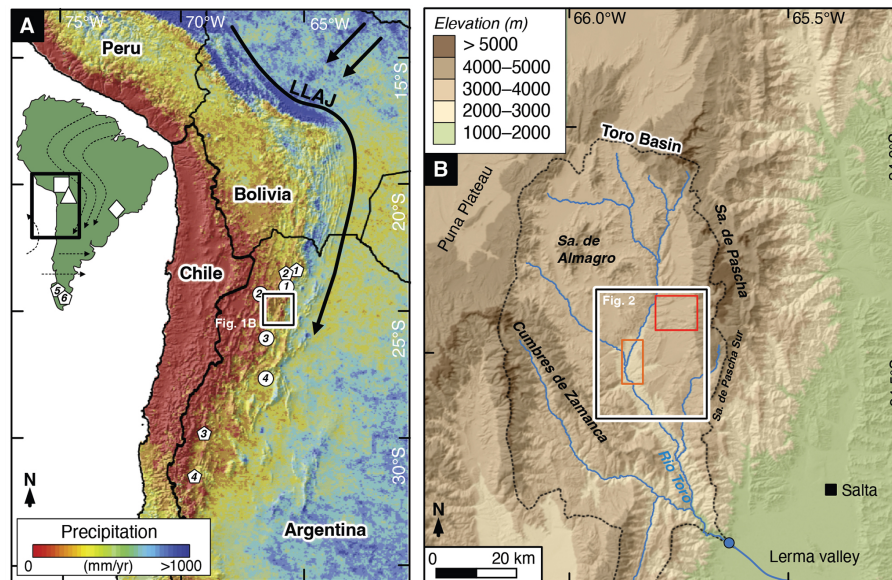
Figure 1. Overview of the topography, rainfall, and moisture transport of the central Andes. **(a)** Tropical Rainfall Measuring Mission rainfall map (TRMM2B31) (Bookhagen and Strecker, 2008). Moisture is transported (black arrows) from Atlantic sources during the South American Summer Monsoon (SASM) by the Low-Level Andean Jet (LLAJ; Vera et al., 2006). The Toro Basin is outlined by the white–black-bordered box. Circles denote regional glacial record locations: (1) Nevado de Chañi (24.0° S, 65.7° W; Martini et al., 2017), (2) Quevar Volcano (24.4° S, 66.8° W; Luna et al., 2018), (3) Sierra de Quilmes (26.2° S, 66.2° W; Zech et al., 2017), and the (4) Sierra del Aconquija (27.2° S, 66.1° W; D'Arcy et al., 2019a). Pentagons denote Mid-Pleistocene Transition (MPT) geomorphic record locations: (1) Casa Grande Basin (23° S, 66.5° W; Pingel et al., 2019b), (2) Salinas Grandes Basin (23.5° S, 66° W; Pingel et al., 2019b), (3) Iglesia Basin (30.5° S, 69° W; Terrizzano et al., 2017), (4) Calingasta Basin (32° S, 69.5° W; Peri et al., 2022), (5) Río Deseado (47° S, 72° W; Tobal et al., 2021), and (6) Río Santa Cruz (50° S, 73° W; Milanez Fernandes, 2023). The inset map of South America in Fig. 1a indicates the extent and location of the Lake Titicaca (square; Fritz et al., 2007), Salar de Uyuni (triangle; Baker et al., 2001), and Botuverá Cave (diamond; Wang et al., 2007) paleoenvironmental records. Dashed arrows outline the moisture-bearing low-level airflow patterns for South America which are deflected by the Andean topography. **(b)** Topography of the Toro Basin (ca. 4000 km^2, 1500–5900 m a.s.l.) from 12 m resolution TanDEM-X (10 m vertical resolution) elevation data. The basin is outlined by a dashed black line, and the upper basin is delineated by a white–black-bordered rectangle (see Fig. 2). Toro alluvial fans and fluvial terraces are outlined by red and orange rectangles, respectively. The basin outlet and the start of the long profile is shown by the blue circle in Fig. 2. Sa. – Sierra.

This study focuses on a suite of fans that emerge from the tributary catchments of the Sierra de Pascha and are located ~ 30 km upstream from the cut-and-fill terraces recording 100 kyr climate cyclicity described by Tofelde et al. (2017). The Pascha ranges are characterized by meta-sediments of the late Proterozoic–Cambrian Puncoviscana Formation and quartzites and shales of the Cambrian Mesón Group (Schwab and Schafer, 1976; García et al., 2013). Long-term rock uplift rates based on structural reconstructions range between 0.4 and 0.6 mm yr^{-1} (Hilley and Strecker, 2005).

The Middle Miocene Barres sandstone and Agujas conglomerates, interbedded with lava flows, and the Pliocene–Pleistocene Alfarcito conglomerates make up the west-tilted strata, which lay between the fan deposits and the Río Toro (Fig. 2a; Hilley and Strecker, 2005; Mazzuoli et al., 2008). Resistant Barres, Agujas, and Alfarcito units characterize several erosional surfaces that stand ~ 700 m above the modern river channel. Incision into these tectonically deformed units by tributaries draining the Sierra de Pascha is thought to have occurred after 0.98 Ma (Hilley and Strecker, 2005),

the age of an intercalated ash unit dated from the uppermost layers of the Alfarcito Conglomerate (Marrett et al., 1994). Undeformed Quaternary conglomerates (also called "terrace conglomerates") and fluvial/alluvial deposits either mantle or infill this tectonically deformed and eroded paleotopography (Fig. 2; Marrett and Strecker, 2000; Hilley and Strecker, 2005). The Río Toro sets the local base level for the Pascha tributaries today (Tofelde et al., 2017).

2.2 Climatic setting

Moisture mainly governed by the South American Summer Monsoon (SASM) system is directed by the Low-Level Andean Jet (LLAJ) from the Atlantic Ocean and Amazon basin to the central Andes (Vera et al., 2006; Alonso et al., 2006; Bookhagen and Strecker, 2008; Castino et al., 2017). The semi-arid Toro Basin is located towards the southern limit of this moisture conveyor and receives rainfall that ranges from ~ 900 mm yr^{-1} at the outlet to < 200 mm yr^{-1} in the basin headwaters (Fig. 1; Bookhagen and Strecker, 2008).
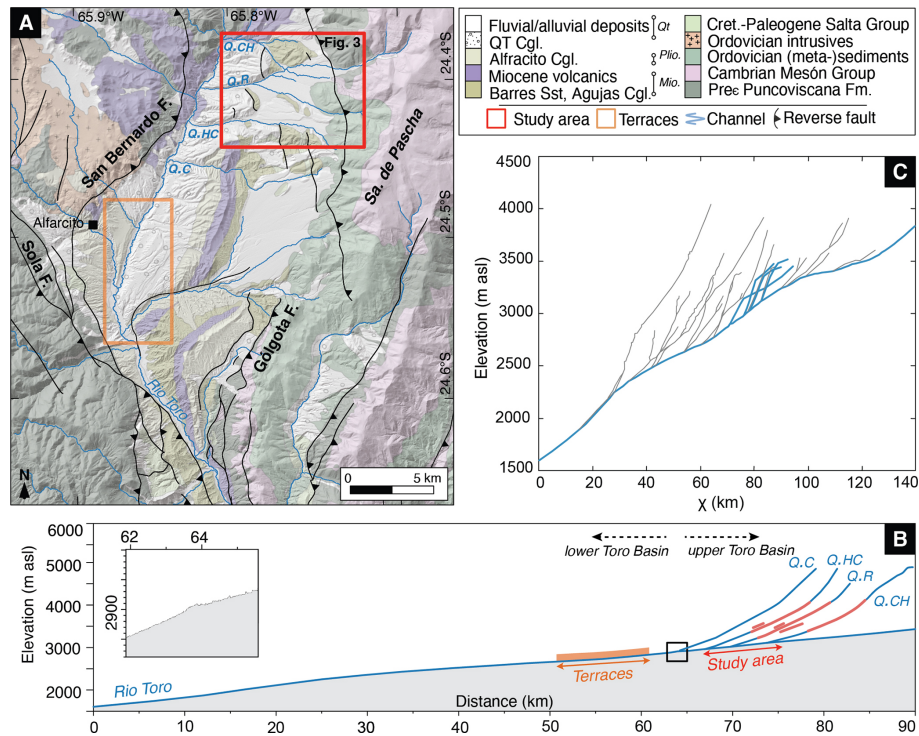
Figure 2. Geology and topography of the upper Toro Basin. **(a)** Geologic map with the alluvial fan sequence location (our study area, Fig. 3) and cut-and-fill terraces described by Tofelde et al. (2017) outlined by red and orange rectangles, respectively. Other terraces extend discontinuously along the basin's channel length but remain undated. Map adapted from SEGEMAR 250 k geological maps and Pingel et al. (2020). Abbreviations: Sa. – Sierra, F – Fault, Q.CH – Quebrada (mountain stream) Chacra Huaico, Q.R – Quebrada Rosal, Q.HC – Quebrada Huasa Ciénaga, Q.C – Quebrada del Chorro, Q.Ca – Quebrada Carachi, Fm – Formation, Cgl – Conglomerates, Sst – Sandstone. **(b)** Long profile of Toro Basin with tributary profiles of upper-basin study area. Upper- and lower-basin reaches are indicated by dashed arrows. Full basin profile extracted from fluvial network outlined in Fig. 1. Alluvial fan and terrace surfaces are projected onto profiles. Inset: higher-resolution plot of proposed knickzone at confluence between the Río Toro and Quebrada del Chorro (outlined in main plot by black box). **(c)** Chi-plot of all channels with a minimum drainage area of $1\,km^2$ within the Toro Basin using a reference concavity index of 0.45. Bold lines highlight the main river channel and tributary catchments within our study area.

The Sierra de Pascha acts as an orographic barrier, causing the eastern flanks of the range to be comparatively wetter than the basin interior. The intensity of the SASM and resultant moisture supply to the central Andes has been variable over time (see Baker and Fritz, 2015, for detailed review). Paleoenvironmental records from Argentina, Chile, and Bolivia show that SASM precipitation has varied with changes in insolation over 19 to 25 kyr (precession) (Godfrey et al., 2003, Fritz et al., 2004, 2010; Placzek et al., 2006; Bobst et al., 2001) and 100 kyr (eccentricity) (Fritz et al., 2007; Gosling et al., 2008) cycles. The central Andes are also subject to increased rainfall during periods of Northern Hemispheric cooling, whereby the Atlantic part of the Intertropical Convergence Zone (ITCZ) is forced southward, bringing moisture with it (Broccoli et al., 2006; Mosblech et al., 2012; Novello et al., 2017; Crivellari et al., 2018). These cold and wet conditions correlate with phases of glacial advance and rising lake levels (Haselton et al., 2002; Vizy and Cook, 2007; Martin et al., 2018; Mey et al., 2020).

Successions of glacial moraines are preserved within the Sierra de Pascha tributary catchments and are indicative of repeated late Quaternary glaciations (Tofelde et al., 2018). Glacial records proximal to the Toro Basin (24–27.2° S) underline the sensitivity of Andean glaciers to SASM precipitation intensity and temperature (Martini et al., 2017; Zech et al., 2017; Luna et al., 2018; D'Arcy et al., 2019a; Mey et al., 2020). The timing of regional glacial stages is invariably in phase with insolation cycles, periods of SASM strengthening, and/or Northern Hemispheric events (e.g., Younger Dryas, Last Glacial Maximum) (D'Arcy et al., 2019a).

2.3   Basin sediment infilling and incision

Thick successions of sediment, together with subtle knickzones and hairpin turns in the Río Toro, reflect a complex late Cenozoic history of basin filling and evacuation (Strecker et al., 2009; Hain et al., 2011; Vezzoli et al., 2012; Pingel et al., 2020), base-level perturbations and tectonic deforma-

tion (Marrett and Strecker, 2000; Hilley and Strecker, 2005; Tofelde et al., 2017), and drainage reorganization (Seagren and Schoenbohm, 2021; Seagren et al., 2022). Given our interest in the Quaternary deposits of the upper Toro Basin, we focus our attention on how the basin has evolved over the last 1 million years.

After deposition of the Alfarcito conglomerates concluded at ca. 0.98 Ma, the Toro Basin was evacuated to a base level lower than today (Hilley and Strecker, 2005). Renewed hydrological connectivity between the Toro Basin and the Lerma Valley likely caused widespread basin sediment evacuation and incision of the (paleo)topography. Uplift of the Sierra de Pascha Sur also recommenced sometime after ca. 0.98 Ma (Hilley and Strecker, 2005). The newly uplifted range impeded the delivery of precipitation to the basin interior, and, by ca. 0.8 Ma, the semi-arid conditions of today were established (Kleinert and Strecker, 2001; Strecker et al., 2007; Pingel et al., 2020). The mechanically strong basement rocks, and a potentially reduced sediment transport capacity, meant that incision was unable to keep pace with the renewed rock uplift. This forced widespread aggradation and a decrease in relief upstream of the Gólgota fault and channel steepening within the bedrock gorge cutting through the Sierra de Pascha Sur (Fig. 2; Hilley and Strecker, 2005; Strecker et al., 2009; García et al., 2013). External drainage either became restricted or ceased at this time (Marrett et al., 1994; Hain et al., 2011; Pingel et al., 2019a). Evidence for a similar sequence of events is seen in the Humahuaca, Casa Grande, and Calchaquí basins (23° S), where renewed range uplift reduced hydrological connectivity and caused sediment infilling (Robinson et al., 2005; Hain et al., 2011; García et al., 2013; Pingel et al., 2013, 2016, 2019a; Streit et al., 2017; Seagren et al., 2022). Although there are some uncertainties about the exact timing, connectivity between the Toro Basin and the foreland is thought to have been re-established due to external base-level change (Seagren and Schoenbohm, 2021).

The Quaternary "terrace conglomerates" were deposited within the Toro Basin starting from ca. 0.94 Ma and are considered part of this phase of uplift-induced basin infilling (Hilley and Strecker, 2005). A flight of six fluvial terrace levels in the lower basin is preserved between 20 and 200 m above the modern Río Toro (Fig. 2). Cosmogenic exposure-age dating of terraces, burial dating of the sediments, and zircon U–Pb ages of intercalated ashes from the terrace levels revealed multiple 100 kyr cut-and-fill sedimentary cycles starting from ca. 500 ka (Tofelde et al., 2017). The phases of incision correspond with cold, wet glacial periods, when sediment transport capacity apparently exceeded sediment flux, whereas aggradation occurred when sediment transport was considerably reduced (Tofelde et al., 2017). Moreover, the calculated net incision rate through the terrace sequence of 0.4 mm yr^{-1} from ca. 500 ka is consistent with long-term rock uplift rates of the Sierra de Pascha Sur (Hilley and Strecker, 2005). Tofelde et al. (2017) thus concluded that,

while the renewed uplift of the Sierra de Pascha Sur helped initiate the deposition of the terrace conglomerates, the periodicity of the cut-and-fill cycles is best explained by orbitally driven climate forcing, with net incision likely associated with the channel response to ongoing rock uplift. Today, catchment-averaged erosion rates for catchments draining the Sierra de Pascha range between < 0.03 and 0.12 mm yr^{-1} (Tofelde et al., 2018).

3 Methodology

To evaluate past channel behavior and landscape response to climate and/or tectonic forcing for the upper Toro Basin, we applied CRN exposure dating to the suite of fan surfaces along the western front of the Sierra de Pascha (Figs. 1 and 2).

Alluvial fan CRN ages record the timing of active sediment deposition or surface stability between periods of channel avulsion and incision (Dühnforth et al., 2007; D'Arcy et al., 2019b), which lead to abandonment of the fan surface. This abandonment can occur due to changes in sediment supply (Brooke et al., 2018; Tofelde et al., 2019), tectonic deformation and base-level change (Ganev et al., 2010; Mouslopoulou et al., 2017), climate-induced changes in water discharge (Steffen et al., 2010; Savi et al., 2016), or drainage reorganization (Bufe et al., 2017). Because fan surfaces can remain active for 10^2–10^5 years before being incised (Cesta and Ward, 2016; Dühnforth et al., 2017; Ratnayaka et al., 2019; Peri et al., 2022), the age distribution or minimum exposure age of boulders on an alluvial fan surface will not necessarily tightly constrain the timing of abandonment. Instead, the distribution of CRN ages, after excluding clear outliers, more likely reflects phases of fan activity and, at best, provide a minimum age limit for the onset of incision leading to eventual surface abandonment (D'Arcy et al., 2019b).

We mapped the upper Toro Basin fans using TanDEM-X (12 m resolution) data and Google Earth imagery. The stratigraphic relationships among the different fan surfaces were used to inform the cosmogenic radionuclide (CRN) sampling strategy (e.g., McFadden et al., 1989; Hughes et al., 2010; Hedrick et al., 2013).

Supporting topographic, fan, and channel data were extracted from the digital elevation model (DEM) using Topo-Toolbox functions in MATLAB (Schwanghart and Scherler, 2014) and geospatial toolboxes (GRASS, GDAL) in QGIS (geographic information system software). We also compiled a set of climate (Berger and Loutre, 1991; Baker et al., 2001; Imbrie and McIntyre, 2006; McIntyre and Imbrie, 2000; Fritz et al., 2007; Wang et al., 2007; Lisiecki and Raymo, 2009), paleoenvironmental (Hilley and Strecker, 2005; Tofelde et al., 2017; Pingel et al., 2020), glacial (Martini et al., 2017; Zech et al., 2017; Luna et al., 2018; D'Arcy et al., 2019a; Mey et al., 2020), and geomorphic (Terrizzano et al., 2017; Tofelde et al., 2017; Pingel et al., 2019b; To-

bal et al., 2021; Peri et al., 2022; Milanez Fernandes, 2023) records for the Andes to help contextualize our results.

3.1 CRN dating

We collected a total of 30 quartzite boulder surface samples from eight fan surfaces (Fig. 3). Between three and four boulders were sampled per surface. Each surface was named "Qf" for "Quaternary fan", followed by a number which referred to its stratigraphic position. For example, Qf_1 sits ~ 200 m above the modern river channel, and, as the highest elevation surface of the study area, it was anticipated to be the oldest fan.

Each sampled boulder was embedded within the fan surface, located away from channels, and within the distal zone of the landform. This sampling strategy reduced the likelihood that the boulders were sourced from adjacent hillslopes or were part of a depositional event following landform abandonment (D'Arcy et al., 2019b; Orr et al., 2021). The sampled boulders were the largest, freshest boulders that we were able to identify within the distal zone. However, we cannot definitively discount the possibility that the boulders experienced some weathering, surface spallation, or fracturing in the past.

We removed between 400 and 1000 g of sample from the upper 3 cm of each boulder surface. The samples were crushed and then sieved to isolate the 250–500 µm grain size fraction needed for CRN dating. Sample cleaning, purification, carrier addition, extraction and oxidation of Be, and target preparation for AMS measurement were conducted in the Helmholtz Laboratory for the Geochemistry of the Earth Surface (HELGES) at the German Research Centre for Geosciences (GFZ-Potsdam) using the procedures outlined by von Blanckenburg et al. (2004) and Wittmann et al. (2016). AMS measurements were completed at the Cologne AMS facility at the University of Cologne, Germany.

Exposure ages derived from in situ-produced ^{10}Be concentrations were calculated using the CREp online calculator (Martin et al., 2017) with the regional reference (at sea level and high latitude (SLHL)) production rate of 3.74 (± 0.09) at g^{-1} yr^{-1} for the high-elevation (> 3400 m a.s.l.) central Andes (Blard et al., 2013; Kelly et al., 2015; Martin et al., 2015) and the Lifton–Sato–Dunai (LSD) scaling scheme (Lifton et al., 2014). Further information about the boulder samples and the CRN laboratory procedure, blank ratios, and age calculation is provided in Figs. S1 and S2 in the Supplement.

The probabilistic model for inferring the timing of fan surface abandonment from D'Arcy et al. (2019b) was applied to fans with exposure ages of less than ca. 300 ka. The model uses the exposure ages of boulders on the fan surface to generate a probability distribution of abandonment ages and a most probable abandonment age. The modeled abandonment age is based on the premise that an alluvial fan surface remains active for a period of time that may generate a range of exposure ages exceeding the uncertainty bounds on any individual age. The calculated abandonment age and its uncertainty is thus dependent on the youngest measured exposure age, the duration of surface activity, and the number of samples. For a detailed description of the approach, see D'Arcy et al. (2019b). The model was not applied to older fan surfaces, which have large age distributions (> 100 kyr range) and likely have some inheritance and/or surface erosion (Phillips et al., 1990; Tobal et al., 2021). Working with chronological data at this coarse resolution over 10^5–10^6-year timescales means that even the most sophisticated inheritance/erosion models are limited in their ability to estimate the timing of landform abandonment (e.g., Prush and Oskin, 2020; Dortch et al., 2022). For the Toro fans where this applies, we use the age distribution, the stratigraphic order of the fans, and the youngest exposure age as a guide for the timing of abandonment.
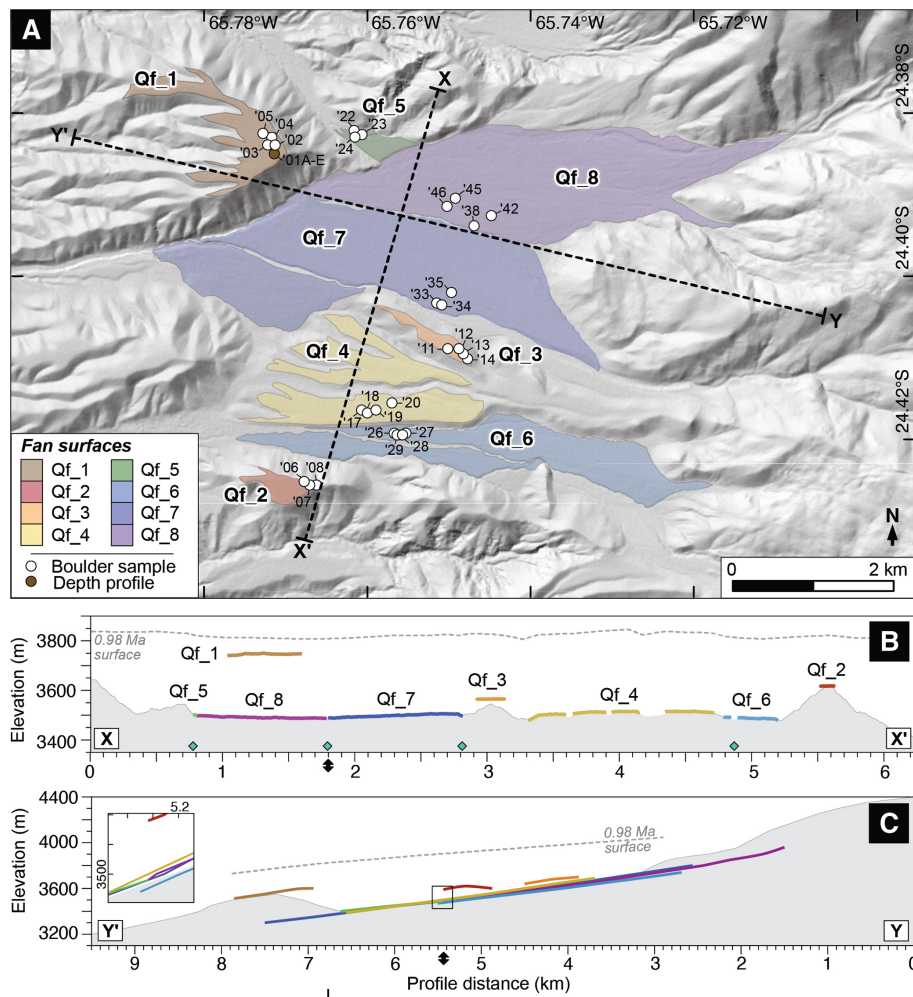
3.2 ^{10}Be depth profile

To help substantiate our new ^{10}Be boulder dataset, we also resampled the Qf_1 ^{10}Be depth profile, referred to as P6b by Tofelde et al. (2017) and corresponding to their terrace level T6. The original profile was limited to five samples, which were sampled over relatively broad depth intervals (0–10, 18–28, 25–81, 82–164, 164–210 cm). To obtain more highly resolved ^{10}Be data for this surface, particularly in the upper 100 cm, five samples of > 65 pebbles each were extracted from the following depth intervals (cm): 0–10, 20–30, 40–50, 60–70, and 115–125. The pebble samples were crushed and sieved, and the 500–1000 µm fraction was reserved for CRN dating. Subsequent laboratory procedures followed those of the boulder samples.

The Qf_1 ^{10}Be depth profile, using combined ^{10}Be data from this study and from Tofelde et al. (2017), was used to determine an exposure age using the Hidy et al. (2010) Monte Carlo simulator. Further details are provided in Figs. S1 and S2.

4 Results

We use the upper Toro Basin alluvial fan elevations, surface characteristics, and CRN ages to identify two generations of fan surfaces. The studied fans are predominantly matrix-supported conglomerates with sub-angular to rounded pebble and cobble clasts. Weathered desert pavements cap many of the fan surfaces; a layer of finer sands and gravels is overlain by pebbles, cobbles, and boulders (e.g., McFadden et al., 1989; Tofelde et al., 2017).

The Generation 1 (G1) fan surfaces, comprising Qf_1 through 4, are stratigraphically the highest in the record and are positioned ~ 200 to 50 m above the modern river channel(s) (Fig. 3). The fan surfaces are moderately to highly weathered, with some evidence of surface boulder spallation (Fig. 4). With a few rare exceptions, the G1 sampled boul-

Figure 3. Alluvial fan surfaces of the upper basin. **(a)** Hillshade map of the dated fan surfaces with boulder and depth profile sampling locations shown. Sample names have been abbreviated (e.g., TB19_05: '05). X–X' and Y–Y' linear projection lines of Fig. 3b and c are represented by dashed black lines. **(b)** Fan sequence stratigraphy shown by fan surfaces projected onto X–X'. Qf_2 and Qf_3 surface widths are slightly exaggerated to improve visibility. Modern topography shaded in gray. The 0.98 Ma surface (dashed gray line) is modeled from sediment evacuation estimates of Hilley and Strecker (2005). Location of active fluvial channels indicated by green diamond symbol. **(c)** Fan surfaces projected onto Y–Y'. Inset plot provides higher-resolution view of projections (outlined by black rectangle). Projection line intersection is indicated by black double arrow.

ders are smaller than those sampled from the lower Generation 2 (G2) surfaces. The G1 and G2 boulders have *b*-axis lengths which range from 30 to 80 cm and 30 to 140 cm, respectively (Fig. S2). The CRN exposure ages from the G1 surfaces range between ca. 970 and 340 ka (Table 1; Figs. 5 and 6).

G2 comprises fans Qf_5 through 8, which have surfaces within 10 m elevation of the modern channel(s) (Fig. 3). These moderately weathered surfaces retain debris flow deposits, evidence of past channel avulsion, and sparse human infrastructure (e.g., stone walls). The CRN exposure ages of this younger fan generation range between ca. 100 and 20 ka, with estimated surface abandonment ages after ca. 70 ka (Table 1; Fig. 7).

4.1 Generation 1

Qf_1 is the highest fan surface of the record ($\sim$ 200 m above the modern channel) and extends from the Quebrada Rosal tributary catchment. The fan comprises part of the Quaternary conglomerates, which overlie the Barres sandstone formation (Figs. 2 and 3). The depth profile is composed of four sedimentary units that coarsen with depth: silts and fine sands (0–20 cm), fine-coarse sand (20–60 cm), coarse sand and gravel (60–180 cm), and gravels (> 180 cm). Consistent with the original profile, the new ^{10}Be sample concentrations decrease exponentially with depth (Fig. 5; Table 2). Qf_1 has a Bayesian most probable exposure age of $715.8^{+35}/_{-217}$ ka (2σ upper age: 750.8 ka; 2σ lower age: 498.8 ka) and $0.26 \pm 0.42 \times 10^6$ atoms g^{-1} of inheritance.
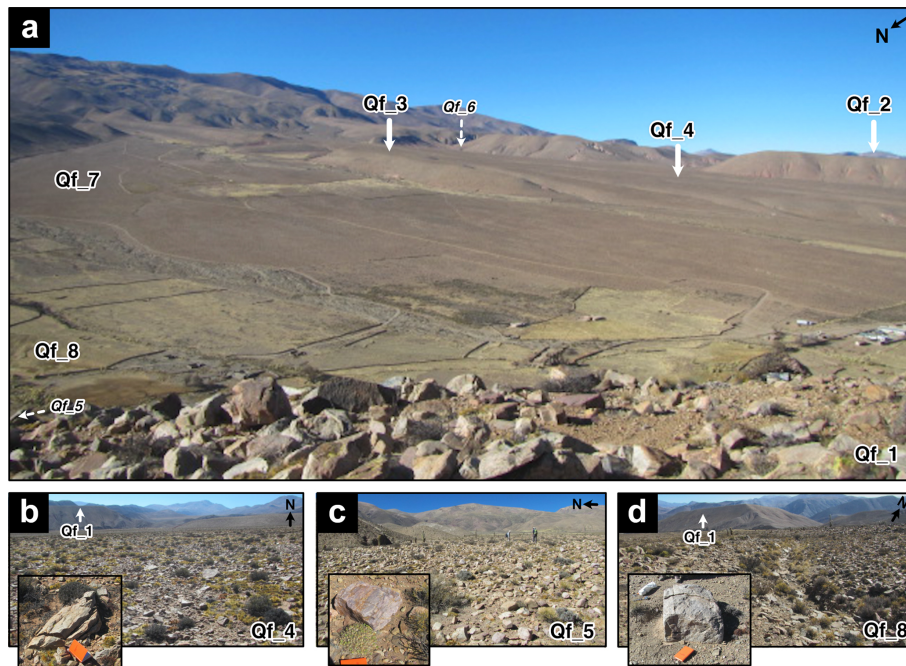
Figure 4. Images of the alluvial fan sequence of the upper Toro Basin. **(a)** Image taken from Qf_1 surface (facing SE) with fan surfaces labeled. Italicized text with arrows indicates the location of surfaces that are not clearly in shot. **(b)** Qf_4 surface. Inset image of sampled boulder TB19_19. **(c)** Qf_5 surface. Inset image of sampled boulder TB19_22. **(d)** Qf_8 surface. Inset image of sampled boulder TB19_44. Panels **(b–d)** encompass the full age range of sampled surfaces. Further images of the fan surfaces and ^{10}Be samples are provided in Fig. S3.

Within the simulator, we constrained fan surface erosion and inflation by setting the erosion rate to range between -0.02 and $0.2\,\mathrm{cm\,ka}^{-1}$ and using maximum and minimum erosion thresholds of -10 and $50\,\mathrm{cm}$, respectively. While this modeled exposure age is consistent with the age estimated earlier by Tofelde et al. (2017) of $732^{+53}/_{-56}$ ka assuming a stable surface, or $644^{+43}/_{-49}$ ka accounting for surface inflation, Tofelde et al. (2017) preferred the exposure age they derived from surface pebbles of 453 ± 33 ka.

The exposure ages of boulder samples TB19_03 and TB19_05 are in agreement with the depth profile results, yielding exposure ages of 639.17 ± 63.94 and 593.11 ± 59.10 ka (2σ uncertainty). The two remaining boulders (TB19_02, TB19_04) yielded older exposure ages of 966.63 ± 109.78 and 884.41 ± 95.34 ka.

Surface Qf_2, the second highest surface (ca. 130 m above the closest modern channel), also overlies the Barres sandstone and likely extends from the Quebrada Huasa Ciénaga and Quebrada del Chorro catchments. CRN exposure ages from three boulders range from 631.88 ± 64.10 to 336.94 ± 33.17 ka.

The Qf_3 surface is positioned ca. 60 m above the closest modern channel and extends from the Quebrada Rosal tributary catchment. The surface yields three CRN boulder exposure ages that cluster between 651.82 ± 66.21 and 533.56 ± 52.88 ka and one younger age of 361.38 ± 35.49 ka.

Qf_4 has a highly dissected fan surface, which is the lowest stratigraphically of the G1 fans; the fan is positioned ca. 40 m below the Qf_3 surface and ca. 30 m elevation above the modern channel. Four boulder exposure ages range from 911.61 ± 100.27 to 548.44 ± 54.60 ka.

4.2 Generation 2

Qf_5 is a small G2 surface that sits ca. 10 m above the neighboring Qf_8 fan. Qf_5 has three exposure ages that range from 98.81 ± 8.82 to 70.63 ± 6.28 ka, with a most probable abandonment age of $61.8^{+13.5}/_{-33.6}$ ka (no ages excluded as outliers).

Qf_6's surface is characterized by moderately weathered debris flow deposits with clusters and elongated ridges of boulders. Exposure ages range between 82.00 ± 7.33 and 69.97 ± 6.27 ka from the four boulders, with an estimated surface abandonment age of $66.2^{+11.0}/_{-17.5}$ ka (no ages excluded as outliers).

Despite Qf_7 being located within 5 m elevation of the youngest G2 fan Qf_8, this large fan appears more weathered than Qf_8. Qf_7 has CRN exposure ages of 66.94 ± 6.13, 59.28 ± 5.35, and 38.78 ± 3.47 ka. The surface abandonment ages including and excluding the youngest age are $33.9^{+7.4}/_{-25.1}$ and $52.9^{+11.0}/_{-16.3}$ ka, respectively.

Surface Qf_8 yielded a cluster of older ages that range between 45.32 ± 4.2 and 43.65 ± 4.04 ka and a single younger age of 22.37 ± 1.83 ka. Abandonment ages includ-

Table 1. Sample properties, measured in situ ^{10}Be concentrations (at g^{-1} SiO$_2 \pm 1\sigma$), and calculated exposure ages (ka $\pm 1\sigma$) of each sampled boulder from the Toro fans. Further sample and age calculation details are provided in Figs. S2 and S3.

Sample	Location			Sample	Shielding	Be-10 concentration		Be-10 exposure ages*	
	Latitude (°S)	Longitude (°W)	Elevation (m a.s.l.)	thickness (cm)	correction	Concentration (10^6 at g^{-1} SiO$_2$)	Uncertainty (10^6 at g^{-1} SiO$_2$)	Age (ka)	Uncertainty (ka)
Qf_1									
TB19_02	−24.38492	−65.76890	3556	1	0.990	24.20	0.78	966.63	109.78
TB19_03	−24.38492	−65.76890	3556	1	0.990	16.02	0.52	593.11	59.10
TB19_04	−24.38492	−65.76890	3556	1	0.990	22.33	0.72	884.41	95.34
TB19_05	−24.38492	−65.76890	3556	1	0.990	16.97	0.55	639.17	63.94
Qf_2									
TB19_06	−24.42522	−65.76775	3560	1	0.999	11.36	0.37	391.94	37.91
TB19_07	−24.42566	−65.76682	3570	2	0.999	17.00	0.55	631.77	64.10
TB19_08	−24.42568	−65.76607	3581	2	0.999	10.18	0.33	336.94	33.17
Qf_3									
TB19_11	−24.40882	−65.75023	3644	1	0.998	15.45	0.50	533.56	52.88
TB19_12	−24.40918	−65.74864	3658	3	0.998	18.06	0.59	651.82	66.21
TB19_13	−24.40976	−65.74810	3660	3	0.998	17.77	0.58	634.67	64.63
TB19_14	−24.41011	−65.74773	3673	3	0.998	11.18	0.37	361.38	35.49
Qf_4									
TB19_17	−24.41665	−65.76059	3509	1	0.999	14.73	0.48	548.44	54.60
TB19_18	−24.41675	−65.76000	3512	2	0.999	17.26	0.56	679.67	68.23
TB19_19	−24.41654	−65.75923	3519	3	0.999	19.06	0.61	778.81	79.15
TB19_20	−24.41533	−65.75681	3541	1	0.999	21.41	0.69	847.34	90.30
Qf_5									
TB19_22	−24.38245	−65.76145	3404	2	0.990	2.02	0.07	70.63	6.28
TB19_23	−24.38263	−65.76109	3407	2	0.995	2.34	0.08	82.69	7.35
TB19_24	−24.38275	−65.76144	3405	3	0.995	2.77	0.09	98.81	8.82
Qf_6									
TB19_26	−24.41923	−65.75623	3531	2	0.998	2.16	0.07	69.97	6.27
TB19_27	−24.41921	−65.75578	3532	1	0.998	2.52	0.08	81.85	7.31
TB19_28	−24.41924	−65.75569	3541	2	0.998	2.22	0.08	71.11	6.46
TB19_29	−24.41941	−65.75652	3525	3	0.998	2.47	0.08	82.00	7.33
Qf_7									
TB19_33	−24.40346	−65.75108	3557	1	0.998	1.22	0.04	38.78	3.46
TB19_34	−24.40371	−65.75107	3555	2	0.998	1.87	0.06	59.28	5.36
TB19_35	−24.40203	−65.74977	3563	3	0.998	2.11	0.07	66.94	6.13
Qf_8									
TB19_38	−24.39402	−65.74711	3533	1	0.997	1.43	0.05	44.34	4.08
TB19_42	−24.39275	−65.74500	3553	1	0.997	1.43	0.05	43.65	4.04
TB19_45	−24.39043	−65.74940	3510	1	0.997	0.63	0.02	22.37	1.85
TB19_46	−24.39140	−65.75027	3502	1	0.997	1.44	0.05	45.32	4.21

* LSD scaling scheme (Lifton et al., 2014), ERA-40 atmosphere model (Uppala et al., 2005), LSD framework for geomagnetic correction (Lifton et al., 2014). Reference (SLHL) production rate: $3.74 + 0.09$ at g^{-1} yr^{-1}. Sample density: 2.75 g cm^{-3}. Erosion: 0 mm yr^{-1}.

ing and excluding the youngest age are $19.4^{+4.1}/_{-19.4}$ and $42.4^{+6.5}/_{-7.5}$ ka, respectively. The surface is covered with relatively unweathered debris flow deposits and large varnish-free boulders.

5 Discussion

While there are some nuances to the Toro Basin fan record, our new CRN dataset enables us to identify significant phases of net incision since ca. 0.98 Ma, capture the channel response to external forcing over a range of timescales and
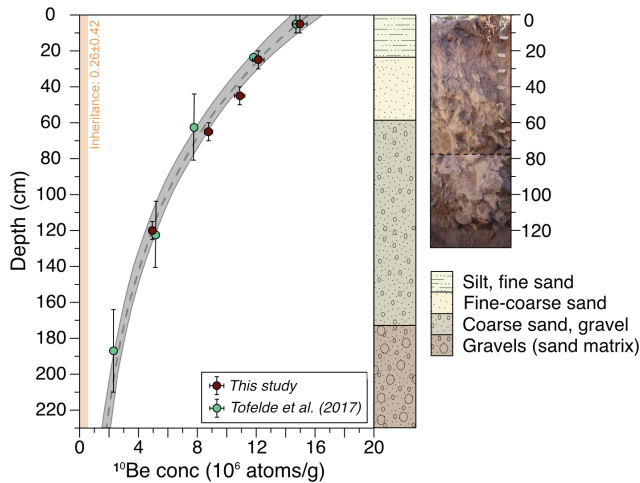
Figure 5. ^{10}Be concentration (10^6 at g^{-1} SiO$_2 \pm 1\sigma$) with depth for Qf_1 profile alongside sedimentary log and stitched field image of the profile pit. Each sample was collected over a depth range represented by a vertical error bar. The horizontal error bar represents the 1σ analytical uncertainty for the nuclide concentration. The Hidy et al. (2010) Monte Carlo simulator fit 100 000 curves (gray shading) to the profile and generated the most probable fit (dashed gray line). Modeled inheritance is shown by the orange line. Profile 6b, rather than 6a, data from the Supplement are used in the simulation due to the mislabeling of the profile in Fig. 4 of Tofelde et al. (2017).

Table 2. Sample depths and measured ^{10}Be concentrations (at g^{-1} SiO$_2 \pm 1\sigma$) of Qf_1 depth profile. The fan age calculated with the Hidy et al. (2010) Monte Carlo depth profile simulator was $715.8^{+35}/_{-217}$ ka. The inheritance measured was $0.26 \pm 0.42 \times 10^6$ at g^{-1} SiO$_2$.

Sample*	Sample depth		Be-10 concentration	
	Depth (cm)	Uncertainty (cm)	Concentration (10^6 at g^{-1} SiO$_2$)	Uncertainty (10^6 at g^{-1} SiO$_2$)
BBC-0	5	5	14.70	0.18
TB19_01A	5	5	14.97	0.48
BBC-1	23	5	11.80	0.11
TB19_01B	25	5	12.14	0.39
TB19_01C	45	5	10.88	0.35
BBC-2	53	28	7.76	0.07
TB19_01D	65	5	8.76	0.28
TB19_01E	120	5	4.94	0.16
BBC-3	123	41	5.21	0.06
BBC-4	187	23	2.30	0.03

* TB19_01A-E from this study. "BBC-1-4" from Tofelde et al. (2017).

cyclicities, and gain further insight into the late Quaternary evolution of the Toro Basin.

5.1 Timing of alluvial fan development and abandonment

CRN age uncertainties on the order of 10^4–10^5 years and a wide range of fan exposure age distributions on individual surfaces present some challenges when interpreting the Toro fan chronostratigraphy, which is crucial for comparison with potential external forcing conditions. Constraining the geological uncertainties of the CRN ages, particularly for old fan surfaces, is often challenging (Owen et al., 2014). For this reason, we use geological, topographic, and paleoenvironmental data alongside the ^{10}Be data to interpret the alluvial fan record. The coarse resolution of the G1 ^{10}Be record means that, while we can reflect upon long-term shifts in channel behavior for the upper Toro Basin, we must exercise caution when linking this record to specific forcing or events (Gray et al., 2014; Dühnforth et al., 2017; Orr et al., 2021). Pairing the ^{10}Be record with cosmogenic ^{21}Ne in the future may help to decipher some of the complexities in the exposure histories of the boulders; ^{21}Ne is well suited for quantifying long-term landscape change in arid, low-erosion environments (Dunai et al., 2005; Ma and Stuart, 2018).

5.1.1 Fan Generation 1

The ~ 200 m elevation difference between the highest and lowest fan surface among Generation 1 means that the G1 surfaces could not have been active simultaneously (Fig. 6). Substantial inheritance and/or erosion has therefore likely affected individual boulders from these surfaces and offers one explanation for the broad spread in ages (> 400 kyr) for each.

Pairing the Qf_1 ^{10}Be depth profile with the surface boulder exposure ages means that we can more robustly constrain the oldest phase of fan development within the study area and use it as a benchmark when evaluating the remainder of the G1 fan record. The most recent phase of Qf_1 surface activity and/or stability is constrained by the depth profile data and two boulders to between ca. 750 and 600 ka. In this case, we believe that CRN inheritance may explain why the remaining two boulders (TB19_02, TB19_04) from this surface yield exposure ages that exceed ca. 800 ka. Considering the whole suite of boulder ages for the G1 fans, which mostly exceed 500 ka, we find it unlikely that the age of 453 ± 33 ka (based on surface pebbles) originally reported by Tofelde et al. (2017) for Qf_1 is correct.

Given the stratigraphic positions of Qf_2 and Qf_3, it is unlikely that active streams were present on these surfaces after ca. 400 ka. For this reason, we suggest that the younger ages for these surfaces are the result of erosion. These surfaces also must be older than surface Qf_4, which yielded a youngest age of ca. 550 ka.

Inheritance also likely explains the old (> 750 ka) boulders on Qf_4, which is stratigraphically younger than Qf_1 and cannot have been active at the same time.
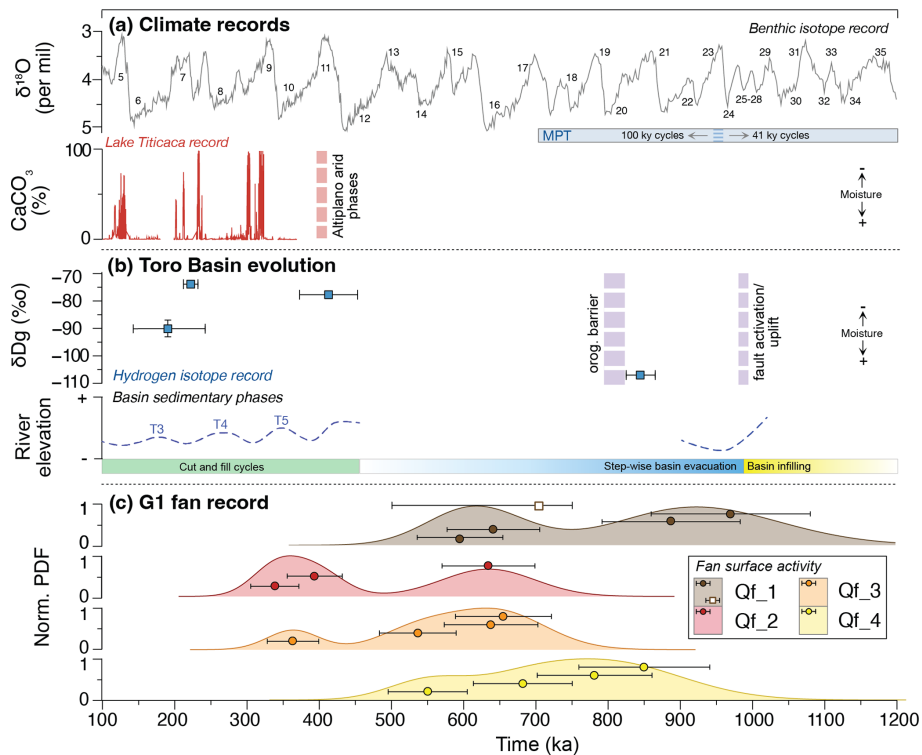
Figure 6. Comparison between the G1 fan [10]Be dataset and records of Toro Basin evolution and climate. **(a)** Benthic isotope record (Lisiecki and Raymo, 2009) displayed alongside Marine Isotope Stage (MIS) and Mid-Pleistocene Transition labeling and the Lake Titicaca sediment core record ($CaCO_3$ concentration) from Fritz et al. (2007). **(b)** Toro Basin evolution. Climatic variability represented by hydrogen isotope record of Pingel et al. (2020). Basin sedimentary and tectonic phases plotted with respect to inferred river elevation over time, as observed by this study and described by Hilley and Strecker (2005), Tofelde et al. (2017), and Pingel et al. (2020). Fluvial terrace record (T3-6) from Tofelde et al. (2017). **(c)** [10]Be surface boulder ages and normalized probability density functions (PDFs) of the G1 surfaces. Horizontal error bars represent the 1σ uncertainty for the exposure ages. The Bayesian modeled surface age of Qf_1 ($715.8^{+35}/_{-217}$ ka) derived from the depth profile (Fig. 5) is denoted by a square point.

Given these complexities in the fan chronostratigraphy, rather than identifying discrete phases of aggradation and incision for each fan surface, we suggest that the G1 fan record can instead be used to capture an extended phase of net incision within the Sierra de Pascha tributaries. Crucially, this is unlikely to be continuous incision, but rather a phase of net incision, which was punctuated by the formation of individual surfaces, possibly controlled by higher-frequency climate cyclicity (e.g., 100 kyr). If so, this would imply periods of faster incision through the fill. By comparing the G1 fan record with the modeled paleotopography of Hilley and Strecker (2005), we estimate that ∼ 100 m of net incision (∼ 0.01 mm yr^{-1}) occurred within the upper basin between ca. 0.98 Ma and 800 ka, at which point the Qf_1 surface became active (Figs. 3b, c and 8). Approximately 200 m of net incision (∼ 0.07 mm yr^{-1}) then followed between ca. 800 ka, and the complete abandonment of the G1 fans followed by ca. 500 ka (when adjusting for age outliers) (Fig. 6), which signals the significant stepwise evacuation of sediment from the upper Toro Basin at this time.

5.1.2 Fan Generation 2

The G2 record reveals that, after a hiatus in the geomorphic record ca. 500 and 100 ka, fan aggradation and incision is recorded throughout several of the Sierra de Pascha tributaries (Fig. 8). Rather than recording continuous fan activity since ca. 110 ka, the distribution of ages for G2 instead likely captures multiple distinct phases of deposition. The G2 fan surfaces have much tighter constrained age distributions (ca. 21 to 40 kyr) compared to the G1 fans, with two G2 fans showing what may be young outliers; the boulders are therefore less likely to be affected by inheritance, but the young outliers may be affected by erosion or tilting by human or animal activity.

5.2 Drivers of alluvial channel system change and fan/terrace formation

Before we can explore some of the possible explanations for the alluvial system change recorded in the Toro Basin, we must first consider the specific local conditions needed to help explain the G1 (ca. 800 to 500 ka) and G2 (ca. 100
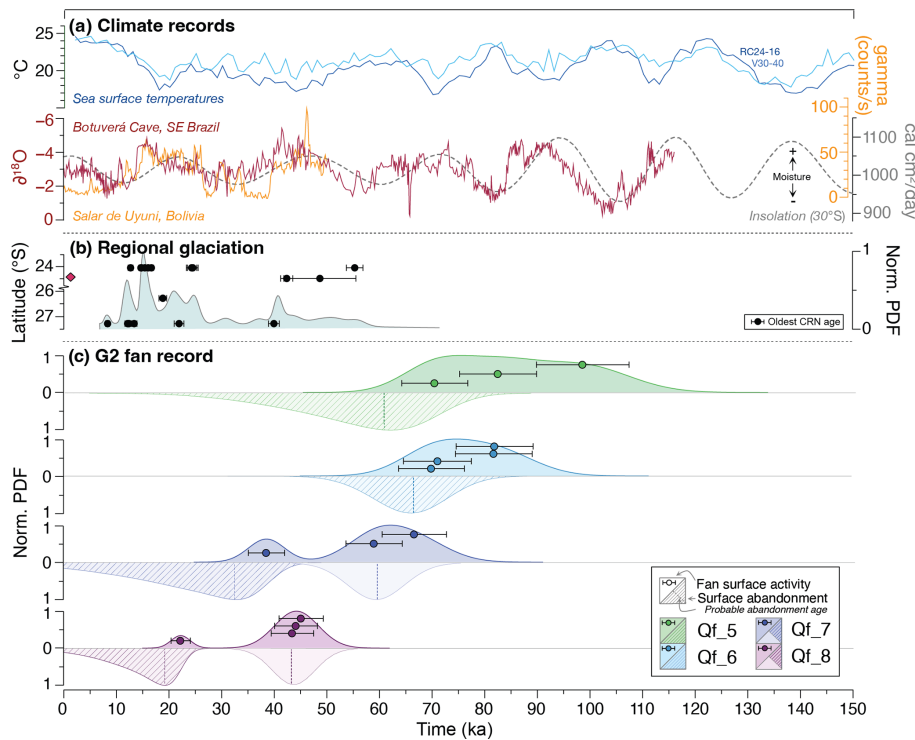
Figure 7. Comparison between the G2 fan ^{10}Be dataset and regional climate and glacial records. **(a)** Climate records. Sea surface temperatures from Imbrie and McIntyre (2006) and McIntyre and Imbrie (2000); insolation from Berger and Loutre (1991); Botuverá Cave, SE Brazil, speleothem record from Wang et al. (2007); and Salar de Uyuni, Bolivia, lake record from Baker et al. (2001). **(b)** CRN glacial chronologies from the central Andes (see Fig. 1a for location): Nevado de Chañi (24° S, 65.7° W; Martini et al., 2017; Mey et al., 2020), Quevar Volcano (24.4° S, 66.8° W; Luna et al., 2018), Sierra de Quilmes (26.2° S, 66.2° W; Zech et al., 2017), and the Sierra del Aconquija (27.2° S, 66.1° W; D'Arcy et al., 2019a). The location of the Toro Basin (24.4° S, 66.7° W) is indicated by a red diamond. **(c)** ^{10}Be surface boulder ages and normalized probability density functions of the G2 surfaces. Horizontal error bars represent the 1σ uncertainty for the exposure ages. Normalized PDF of fan surface abandonment (hashed shading) calculated using the D'Arcy et al. (2019b) probabilistic model for fan surface abandonment. The surface abandonment for Qf_7 and Qf_8 without the youngest boulder ages (TB19_33 and TB19_45, respectively) is shown by PDFs with opaque solid shading. The most probable abandonment ages are denoted with dashed vertical lines. Qf_5: $61.8^{+13.5}/_{-33.6}$ ka. Qf_6: $66.2^{+11.0}/_{-17.5}$ ka. Qf_7: ca. $33.9^{+7.4}/_{-25.1}$ ka ($52.9^{+11.0}/_{-16.3}$ ka). Qf_8: $19.4^{+4.1}/_{-19.4}$ ka ($42.4^{+6.5}/_{-7.5}$ ka).

to 20 ka) fan generations in the upper basin and the fluvial terrace sequence (ca. 370 to < 75 ka) in the lower basin. Changes in water or sediment discharge, governed by climate, can affect channel slopes and prompt adjustments to the channel bed elevations through incision or aggradation (Howard, 1982; Wickert and Schildgen, 2019; Tofelde et al., 2019). Nevertheless, net incision is essential to preserving the geomorphic record of aggradation–incision cycles. Otherwise, subsequent aggradational phases are likely to bury earlier landforms. Net incision can occur through the channel response to ongoing rock uplift or base-level fall (Simpson and Castelltort, 2012), the latter of which may include renewed incision through an aggraded sequence of sediment downstream. While autogenic processes, such as channel avulsion and meander cut-offs, may also play a role in channel incision and the formation of discrete fan lobes or terraces (Nicholas and Quine, 2007; Ventra and Nichols, 2014), we consider the scale of channel incision associated with the

features of interest (ranging from ca. 10 to hundreds of meters) to be beyond the scope of purely autogenic behavior. Below, we consider how climate-modulated changes to water and sediment discharge, together with events that can drive net incision, may have helped to generate and preserve multiple generations of fans and terraces within the Toro Basin.

5.2.1 Fan formation from ca. 800 to 500 ka

The development, entrenchment, and eventual abandonment of the G1 fans could be part of the landscape response to enhanced rock uplift of the Sierra de Pascha Sur, starting no later than ca. 800 ka (Fig. 8) (Clarke et al., 2010; Mather et al., 2017; Mouchené et al., 2017). However, another mechanism is likely at play because the average rates of incision between ca. 800 and 500 ka (0.8 mm yr^{-1}), as recorded by the G1 fans, exceed the estimated rock uplift rates of 0.4–0.6 mm yr^{-1} (Hilley and Strecker, 2005), and tectonic uplift
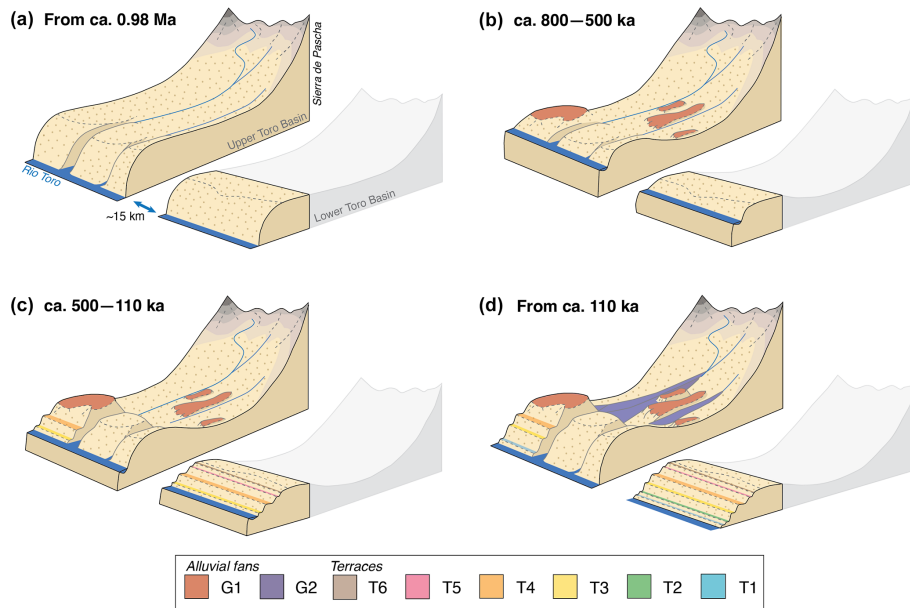
Figure 8. Image illustrating periods of aggradation and incision in the upper and lower Toro Basin from ca. 0.98 Ma (also see Table 3). The area of the lower Toro Basin block shaded in gray was not part of this study. **(a)** From 0.98 Ma: base level lowered to present-day levels, following the deposition of Alfarcito conglomerates. Renewed hydrological connectivity likely led to extensive sediment evacuation and incision of (paleo)topography. Deposition of Quaternary terrace conglomerates started from 0.94 Ma (Hilley and Strecker, 2005). **(b)** ca. 800–500 ka: G1 fan formation and abandonment during a phase of net incision in the upper basin, linked to the MPT. Aggradation was recorded in the lower basin (Tofelde et al., 2017). **(c)** ca. 500–110 ka: 100 kyr cycles of aggradation and incision recorded by lower-basin cut-and-fill terraces (T6 (ca. 490–450 ka), T5 (ca. 370 ka), T4 (ca. 285–260 ka), T3 (ca. 170 ka)). No significant geomorphic change was recognized in the tributaries of the upper basin. **(d)** From ca. 110 ka: G2 fan formation and abandonment in the upper basin, linked to ca. 21/40 kyr climate cycles. Continuation of 100 kyr cycles recorded by lower basin terraces (T2 (ca. 110–75 ka), T1 (< 75 ka)).

Table 3. Summary of upper and lower Toro Basin evolution.

	Upper basin		Lower basin	
	Process/event	Hypotheses (not mutually exclusive)	Process/event	Hypotheses (not mutually exclusive)
From ca. 0.98 Ma (Fig. 8a)	Base level lower than modern	(i) Renewed hydrological connectivity triggers incision	Base level lower than modern	(i) Renewed hydrological connectivity triggers incision
			Deposition of "terrace conglomerates"	(i) Uplift-induced basin infilling
ca. 800–500 ka (Fig. 8b)	Net incision recorded by G1 fan sequence	(i) Enhanced glacial cycles trigger incision (ii) Uplift of Sierra de Pascha Sur	Stability/continued deposition	(i) Lower reaches minimally affected by uplift (ii) System feedbacks promote stability/aggradation (iii) Response time exceeds forcing period
ca. 500–110 ka (Fig. 8c)	No activity recorded	(i) Restricted hydrological connectivity (ii) Downstream incision not yet propagated to upper basin	100 kyr cut-and-fill sedimentary cycles and net incision recorded by fluvial terraces	(i) Eccentricity-driven climate forcing, with continued uplift/base-level drop causing net incision
From ca. 110 ka (Fig. 8d)	G2 fan aggradation–incision cycles and net incision	(i) Surface abandonment during intensified SASM/glacial periods		

alone is unlikely to be pulsed in a manner that would generate multiple fans. More likely, both climate forcing and tectonic forcing combine to produce and preserve the G1 fan sequence. Over the same period, curiously, no terraces are detected in the lower Toro Basin. Three possible explanations for this absence (which are not mutually exclusive) are as follows: (1) due to their more central position within the basin, the lower reaches of the Río Toro were not strongly affected by rock uplift, meaning that any changes in river channel elevation are not persevered in the geomorphic record due to low or a lack of net incision; (2) channels in the lower Toro Basin continued to experience aggradation or remained stable at this time, due to feedbacks in the system whereby incision upstream caused a pulse of sediment for downstream reaches; or (3) the response time of the Río Toro within the lower basin was substantially longer than the forcing period of the aggradation–incision cycles, meaning perturbations to the channel bed elevation due to climate forcing would not have reached so far downstream.

To elaborate on the first possibility, the Sierra de Pascha catchments are positioned behind and perpendicular to west-tilted and deformed basin strata (Barres sandstone, Agujas and Alfarcito conglomerates, lava flows) (Fig. 2a). In concert with the work by Hilley and Strecker (2005), we suggest that channel incision through the resistant sedimentary units accelerated sometime between 0.98 and 0.8 Ma. Once this incision propagated upstream, the removal of weakly consolidated sedimentary units in the upper basin was likely efficient (Hilley and Strecker, 2005). This evolving topography could therefore help to explain the net incision needed in the upper Toro Basin to preserve the alluvial fan surfaces between ca. 800 to 500 ka and why terrace levels in the lower basin are not recognized during this time interval.

To elaborate on the second and third possibilities, as late Quaternary glaciations were limited to the Pascha tributary headwaters (< 5 km from headwall), the hillslope geomorphic response to prolonged and intensified glaciation may have been very localized (Tofelde et al., 2018). This is apparently true for the Iglesia and Calingasta basins in the Western Precordillera, where the tributaries, rather than the main basin, record incision following the Mid-Pleistocene Transition (MPT) (Terrizzano et al., 2017; Peri et al., 2022). Following this argument, the response time of the Río Toro's long profile to the 100 kyr climate cycles after the Mid-Pleistocene Transition (ca. 1.2 to 0.8 Ma) may have been substantially longer than the period of external forcing. If true, this implies that upstream reaches of the channel may have experienced no (or very low-amplitude) aggradation/incision cycles (Allen, 2008; McNab et al., 2023). Alternatively, feedbacks within the system could lead to differences not only in the magnitude of aggradation/incision, but also in the timing. For example, in southwestern Peru, Steffen et al. (2009, 2010) interpreted aggradation in downstream reaches of river channels during past wet climate periods to result from pulses of sediment mobilized from hillslopes and upstream channel incision.

5.2.2 Terrace formation from ca. 500 to 110 ka

From ca. 500 to 110 ka in the upper Toro Basin, we find no record of fan formation (Fig. 8). Curiously, again, though, the lower Toro Basin exhibits a spectacular sequence of terraces showing 100 kyr cyclicity starting from ca. 500 ka (Tofelde et al., 2017). If long channel response times explain the lack of terraces from ca. 800–500 ka in the lower Toro Basin, to explain the terraces identified in the lower basin ca. 500 ka (Tofelde et al., 2017), the channel response time must have changed. This could have occurred as a result of incision in the upper Toro Basin, which would have narrowed the upstream river valleys, consequently decreasing river response times and enabling aggradation–incision cycles to affect channel reaches farther downstream (e.g., McNab et al., 2023).

While a shortened channel response time can explain the formation of terraces in the lower Toro Basin, it does not explain the absence of terraces/fans in the upper basin over the same period. Consequently, we next consider other factors that might lead to differences in fan/terrace preservation between the upper and lower Toro basins.

Perturbations at the Río Toro outlet, such as a shift in base level, will propagate upstream over time, thus driving the net incision needed to preserve variations in channel bed elevation in the terrace and fan sequences. Alternatively, activity along the Gólgota fault at this time may have adjusted the base level for the trunk stream. Regardless of the exact trigger for base-level fall (e.g., renewed fluvial connectivity, possibly enhanced by a drop in the Lerma Valley lake level) (Malamud et al., 1996; González Bonorino and Abascal, 2012), a net incisional wave would have propagated upstream from the lower basin or outlet. That incision would have facilitated terrace preservation in the lower Toro Basin before the incisional wave propagated upstream to the upper Toro Basin. Steepened reaches of both the trunk stream and tributaries up to an elevation of ca. 3400 m (Fig. 2c) are consistent with an upstream-propagating wave of incision, which probably only recently reached the ca. 3300 m elevation of the G2 fan toes.

Consistent with this interpretation, both the upper and lower Toro basins preserve geomorphic evidence of channel bed elevation lowering after ca. 100 ka (terraces T2 and T1 in the lower Toro Basin; G2 fan generation in the upper Toro Basin). While T2 and T1 lie 40 and 20 m, respectively, above the modern Río Toro, the G2 fans are at most 10 m above their closest channel. This finding further supports the idea that net incision is ongoing in the lower Toro Basin, probably keeping pace with the ongoing uplift of the Sierra de Pascha Sur (Tofelde et al., 2017), but net incision has possibly only resumed within the last ca. 110 to 50 kyr in the upper Toro Basin.

Other factors may have also played a role in the misaligned timing of fan/terrace formation in the upper and lower Toro basins. Restricted hydrological connectivity or disconnectivity can lead to internal variability in the nature and timing of a basin's geomorphic or sedimentary response to external perturbations (Fryirs et al., 2007; Buter et al., 2022). For example, basin connectivity and geometry appear to have disrupted the timing of climate-driven sediment transfer within the Humahuaca Basin of NW Argentina during the last glacial cycles, leading to anti-phased timing of aggradation–incision cycles along tributaries on either side of the valley (Schildgen et al., 2016). No fault lines, which can influence connectivity (Guarnieri and Pirrotta, 2008; Brocard et al., 2012), intersect the channel network between the alluvial fans and terrace levels of the Toro Basin (Fig. 2) (Pingel et al., 2020). Nevertheless, minor adjustments to the long profile of an alluvial channel network can be sufficient to affect the internal connectivity of a basin (Savi et al., 2020). One such adjustment may include the tributary junction fan at the Quebrada de Chorro outlet, which has created a diffuse knickzone in the Río Toro long profile (Fig. 2b). As the fan has aggraded, it has pushed the main channel to the opposite valley side, evidenced by a marked channel bend. The fan may therefore inhibit the coupling between the upstream and downstream reaches of the trunk stream by disrupting the flow of sediment and (possibly) water from the Sierra de Pascha tributaries and along the Río Toro (e.g., Harvey, 2012). However, the capacity of the fan to disrupt environmental signals moving through the basin may depend on the direction of signal travel. For example, channel incision due to a climate-induced increase in water discharge may continue to propagate downstream, regardless of a new sedimentary input from a major tributary, unless the tributary fully dams the upstream section. However, if a wave of incision is instead migrating upstream, a tributary junction fan may slow or disrupt its propagation (Savi et al., 2020). Nevertheless, while sedimentary inputs from individual tributaries can affect the modern channel profile and may slow upstream-propagating incisional cycles, it is not clear whether such localized features will play an important role in channel network evolution over longer (e.g., > 100 kyr) timescales.

5.2.3 Fan formation since ca. 110 ka

All G2 surfaces were either stable or actively receiving sediment for some time during both cool, wet glacial periods and warm, dry interglacials. Similar to the terraces in the lower basin (Tofelde et al., 2017), the timing of G2 surface abandonment is restricted to glacial phases; enhanced moisture availability due to an intensified SASM is likely to have amplified sediment transport and channel incision (Baker and Fritz, 2015). Around the latitude of the Toro Basin, glacial moraine records in the central Andes show strong evidence for glacial advances at ca. 16 and 22–24 ka, with some evidence also for advances at ca. 42 and e.g., 20/55 ka (D'Arcy

et al., 2019a; Fig. 7b). The stratigraphically highest surfaces in G2, Qf_5 and Qf_6, show abandonment ages that are consistent with the timing of the oldest glacial advances recorded in the moraine record (ca. 55 ka).

For surfaces Qf_7 and Qf_8, the timing of abandonment is harder to interpret, due to the difficulty in knowing whether the youngest boulders on each surface are outliers due to erosion/rotation or if they represent a time of active deposition on the surface. Given the similarities in surface weathering between Qf_6 and Qf_7, it is possible that Qf_7 was active at the same time as Qf_6 and Qf_5 and hence was abandoned at a similar time (implying that the youngest boulder of Qf_7 is an outlier). If the young boulder instead represents a real depositional age, then the abandonment of Qf_7 could be linked to the ca. 22–24 ka glacial advance, coinciding with the Northern Hemisphere Last Glacial Maximum. The abandonment of Qf_8 is similarly challenging to interpret, with abandonment potentially linked to either the ca. 24 ka glacial advance (associated with the "Minchin" wet climate phase of the central Andes) if the youngest boulder is excluded or the ca. 16 ka glacial advance associated with Heinrich Stadial 1 if not excluded.

While we reason that the two youngest ages from Qf_7 and Qf_8 are not outliers and instead reflect later deposition events (see Sect 5.1.2), we have also estimated the timing of surface abandonment without them (Fig. 7). In this alternative record, the abandonment of three of the four fans falls between ca. 65 and 60 ka. This points to a modest phase of net incision in several Sierra de Pascha catchments during a dry interglacial period (Fritz et al., 2007).

Overall, the exposure age distributions and estimated abandonment ages appear to capture cycles of fan aggradation–incision with relatively high periodicity. Considering the above tentative links between abandonment times and glacial advances and that no known tectonic forcing in the Toro Basin can explain this cyclicity, the alluvial channel network is likely responding to precession- (21 kyr) or obliquity-driven (40 kyr) climate cycles. Precessional forcing has been recorded within the sedimentary archives elsewhere in the central Andes, including fluvial terraces in the Humahuaca Basin (23° S) (Schildgen et al., 2016) and alluvial fans in the Santa María Basin (26.5° S) (D'Arcy et al., 2018) in NW Argentina.

5.3 Impacts of the Mid-Pleistocene Transition on the Toro Basin

The G1 fan surfaces have CRN exposure ages that span several glacial–interglacial cycles (Fig. 6). Although our interpreted ages are too imprecise to associate with specific glacial phases, 100 kyr glacial moderation of aggradation–incision cycles is thought to have controlled fluvial terrace formation in the lower Toro Basin (e.g., Tofelde et al., 2017). In semi-arid landscapes and transport-limited systems, this finding is not unexpected, as geomorphic activity is invari-

ably amplified during wetter glacial periods (Harvey et al., 1999; Spelz et al., 2008; Cesta and Ward, 2016). Given the number of G1 fans ($n = 4$) capturing the prolonged net incisional phase (> 300 kyr), it is possible that eccentricity-driven cycles of aggradation and incision are also recorded in the upper Toro Basin.

Our net incisional phase between ca. 800 and 500 ka coincides with the onset of prolonged and enhanced global glacial cycles following the Mid-Pleistocene Transition (MPT; 1.2–0.8 Ma), which marked a shift in climate periodicity from 41 to 100 kyr cycles (Berger et al., 1999). The southward migration of the ITCZ at this time led to heightened moisture availability throughout the central Andes (Haselton et al., 2002; Broccoli et al., 2006; Vizy and Cook, 2007). Alluvial channels in semi-arid regions of the central Andes are found to respond quickly to marked shifts in precipitation such as this (e.g., Schildgen et al., 2016; Tofelde et al., 2017), which also appear to drive phases of enhanced sediment evacuation to the foreland (Fisher et al., 2023).

Enhanced incision likely linked to the MPT has also been recognized at other locations in the central Andes (Fig. 1a), including the Casa Grande Basin ($23°$ S) in the Eastern Cordillera, the Salinas Grandes Basin ($23.5°$ S) of the Puna Plateau (Pingel et al., 2019b), and the Iglesia ($30.5°$ S) and Calingasta ($32°$ S) basins in the Western Precordillera (Terrizzano et al., 2017; Peri et al., 2022). These observations point to a regional phase of net incision and therefore landscape response to global climate change. For several of these locations, including the Toro Basin, local tectonic activity may have provided a secondary driver for incision or created conditions conducive to fan/terrace preservation. Towards the Andean interior, the geomorphic response to the MPT probably lessens, as moisture and the extent of past glaciations is more restricted (Luna et al., 2018; Haselton et al., 2002). Beyond the central Andes, fluvial terraces along the Río Deseado ($47°$ S) (Tobal et al., 2021) and Río Santa Cruz ($50°$ S) (Milanez Fernandes, 2023), draining the southern Andes in Patagonia, also record a period of net incision that can tentatively be linked to the MPT. On a global scale, a growing number of studies have identified periods of intensified erosion at this time, for example, in the Saint Elias mountains in Alaska (Gulick et al., 2015), Central Appalachia (Del Vecchio et al., 2022), the Rocky Mountains (Pedersen and Egholm, 2013), and the European Alps (Haeuselmann et al., 2007; Valla et al., 2011; Sternai et al., 2013). While it is not possible to entirely discount a tectonic influence on landscape change in the upper Toro Basin due to some chronological ambiguity in the datasets and inherent challenges in deconvolving different forcing mechanisms, the links between MPT climate and incision, and their expression elsewhere in the Andes and beyond, is compelling.
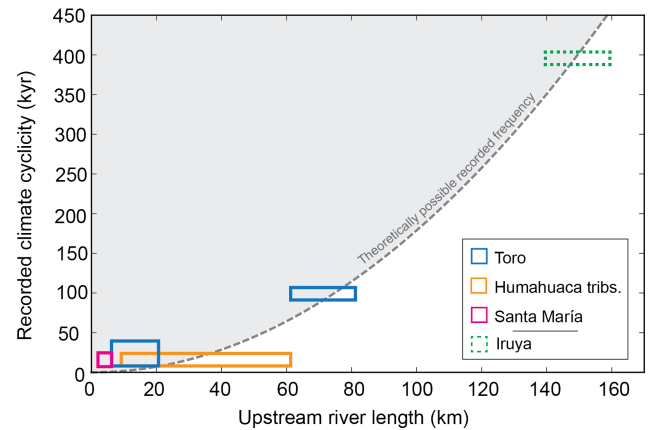
Figure 9. Correlation between recorded climate cyclicity and upstream river length recognized in four basins of the central Andes: Toro (this study; Tofelde et al., 2017), Humahuaca (Schildgen et al., 2016), Santa María (D'Arcy et al., 2018), and Iruya (Fisher et al., 2016). Unlike the other records of aggradation and incision, the Iruya record is derived from the basin's sedimentary record and is a paleo-erosion dataset. Adapted from Tofelde et al. (2017). The recorded period (in kiloyears) is calculated as follows: $0.019 \times$ the square of the river length.

5.4 Climate periodicity and alluvial channel system length

Higher-frequency climate cycles are recorded in fan generation G2 of the Sierra de Pascha tributaries compared with the mainstem of the basin; the alluvial fans, which appear to record climate cycles with a periodicity of ca. 20 to 40 kyr, have an upstream channel length of ~ 10 km and are positioned ~ 30 km upstream of the terrace sequence showing 100 kyr climate cyclicity dated by Tofelde et al. (2017). This finding substantiates the theory that the response time of alluvial channel systems to perturbations in climate depends on system length (Paola et al., 1992; Castelltort and Van Den Driessche, 2003; Godard et al., 2013; McNab et al., 2023). Evidence of this relationship, together with the dependency on the square of the system length, was identified in the archive of several sedimentary basins in the central Andes, although only a single forcing frequency was recorded within each basin (Fig. 9) (Tofelde et al., 2017). Our new data from the Toro Basin provide critical field evidence that multiple climate periodicities can be preserved within the sedimentary record of a single sedimentary basin, with higher forcing frequencies recorded only in the uppermost reaches of the basin.

6 Conclusions

The alluvial fan and terrace sequences of the Toro Basin present an excellent opportunity to explore (1) how channel responses to external perturbations may or may not propagate

downstream and (2) the differences in landscape response to forcing frequency as a function of stream length. We applied CRN dating to a suite of alluvial fan surfaces to characterize the evolution of the alluvial channel network of the Toro Basin over the last 1 million years. Our key findings are as follows:

1. We identified two generations of fan surfaces (G1 and G2) in the Sierra de Pascha tributary catchments. The G1 fans record CRN exposure (^{10}Be) ages between ca. 800 and 500 ka, whereas the G2 fans record surface activity and then abandonment between ca. 100 and 20 ka.

2. The G1 fans capture a significant phase of net incision (~ 200 m) between ca. 800 and 500 ka. The stepwise evacuation of the upper basin coincides with the onset of prolonged and enhanced global glacial cycles following the Mid-Pleistocene Transition (MPT). With several basins in the central Andes and beyond also registering this phase of incision, we propose that the G1 fans are part of a continental-scale response to MPT climate change.

3. The abandonment of the G2 fans is restricted to glacial periods, possibly modulated by 21/40 kyr climate cycles; enhanced moisture availability due to an intensified SASM likely amplified channel incision and sediment transport.

4. Differences in the timing of alluvial fan and fluvial terrace development in the upper and lower Toro basins appear to be associated with how channel length affects fluvial response time to climate forcing and local controls on net incision, which facilitates preservation of the geomorphic record of aggradation–incision cycles.

5. The new alluvial fan record from the upper Toro Basin, combined with earlier results on fluvial terraces from the lower Toro Basin, provides field evidence for the theoretical predictions of a scaling relationship between climate forcing frequency recorded in sedimentary archives and the system length. We show that multiple climate periodicities can be preserved within the sedimentary record of a single sedimentary basin, with higher forcing frequencies recorded only in the uppermost reaches of the basin. This improved understanding of the role of system length in climate signal propagation is an important step forward in helping us to anticipate the spatial distribution of sedimentary paleoclimate records within landscapes.

Code and data availability. Data are available either as part of the main article or within the Supplement. The probabilistic model for fan surface abandonment (D'Arcy et al., 2019b) is available at https://doi.org/10.5194/esurf-7-755-2019-supplement.

Supplement. The supplement related to this article is available online at: https://doi.org/10.5194/esurf-12-1391-2024-supplement.

Author contributions. Conceptualization: ENO, TFS, and ST. Sample collection and processing: ENO, TFS, ST, and HW. Visualization: ENO with feedback from all authors. Writing and editing: all authors.

Competing interests. The contact author has declared that none of the authors has any competing interests.

Disclaimer. Publisher's note: Copernicus Publications remains neutral with regard to jurisdictional claims made in the text, published maps, institutional affiliations, or any other geographical representation in this paper. While Copernicus Publications makes every effort to include appropriate place names, the final responsibility lies with the authors.

Review statement. This paper was edited by Veerle Vanacker and reviewed by Burch Fisher and Gregoire Messager.

References

Allen, P. A.: Time scales of tectonic landscapes and their sediment routing systems, Geological Society, London, Special Publications, 296, 7–28, https://doi.org/10.1144/SP296.2, 2008.

Alonso, R. N.: Estratigrafía del Cenozoico de la cuenca de Pastos Grandes (Puna Salteña) con énfasis en la Formación, Revista de la Asociación Geológica Argentina, 47, 189–199, 1992.

Alonso, R. N., Bookhagen, B., Carrapa, B., Coutand, I., Haschke, M., Hilley, G. E., Schoenbohm, L., Sobel, E. R., Strecker, M. R., Trauth, M. H., and Villanueva, A.: Tectonics, climate, and landscape evolution of the southern central Andes: the Argentine Puna Plateau and adjacent regions between 22 and 30° S, The Andes: Active Subduction Orogeny, 265–283, https://doi.org/10.1007/978-3-540-48684-8_12, 2006.

Armitage, J. J., Dunkley Jones, T., Duller, R. A., Whittaker, A. C., and Allen, P. A.: Temporal buffering of climate-driven sediment flux cycles by transient catchment response, Earth Planet. Sc. Lett., 369–370, 200–210, https://doi.org/10.1016/j.epsl.2013.03.020, 2013.

Baker, P. A. and Fritz, S. C.: Nature and causes of Quaternary climate variation of tropical South America, Quaternary Sci. Rev., 124, 31–47, https://doi.org/10.1016/j.quascirev.2015.06.011, 2015.

Baker, P. A., Rigsby, C. A., Seltzer, G. O., Fritz, S. C., Lowenstein, T. K., Bacher, N. P., and Veliz, C.: Tropical climate changes at millennial and orbital timescales on the Bolivian Altiplano, Nature, 409, 698–701, https://doi.org/10.1038/35055524, 2001.

Berger, A. and Loutre, M. F.: Insolation values for the climate of the last 10 million years, Quaternary Sci. Rev., 10, 297–317, https://doi.org/10.1016/0277-3791(91)90033-Q, 1991.

Berger, A., Li, X. S., and Loutre, M. F.: Modelling northern hemisphere ice volume over the last 3 Ma, Quaternary Sci. Rev., 18, 1–11, https://doi.org/10.1016/S0277-3791(98)00033-X, 1999.

Bernard, T., Sinclair, H. D., Gailleton, B., Mudd, S. M., and Ford, M.: Lithological control on the post-orogenic topography and erosion history of the Pyrenees, Earth Planet. Sc. Lett., 518, 53–66, https://doi.org/10.1016/j.epsl.2019.04.034, 2019.

Blard, P.-H., Braucher, R., Lavé, J., and Bourlès, D.: Cosmogenic ^{10}Be production rate calibrated against ^{3}He in the high Tropical Andes (3800–4900 m, 20–22° S), Earth Planet. Sc. Lett., 382, 140–149, https://doi.org/10.1016/j.epsl.2013.09.010, 2013.

Bobst, A. L., Lowenstein, T. K., Jordan, T. E., Godfrey, L. V., Ku, T. L., and Luo, S.: A 106 ka paleoclimate record from drill core of the Salar de Atacama, northern Chile, Palaeogeogr. Palaeocl., 173, 21–42, https://doi.org/10.1016/S0031-0182(01)00308-X, 2001.

Bonorino, G. G. and Abascal, L.: Drainage and base-level adjustments during evolution of a late Pleistocene piggyback basin, Eastern Cordillera, Central Andes of northwestern Argentina, GSA Bulletin, 124, 1858–1870, https://doi.org/10.1130/B30395.1, 2012.

Bookhagen, B. and Strecker, M. R.: Orographic barriers, high-resolution TRMM rainfall, and relief variations along the eastern Andes, Geophys. Res. Lett., 35, L06403, https://doi.org/10.1029/2007GL032011, 2008.

Brocard, G., Willenbring, J., Suski, B., Audra, P., Authemayou, C., Cosenza-Muralles, B., Morán-Ical, S., Demory, F., Rochette, P., Vennemann, T., and Holliger, K.: Rate and processes of river network rearrangement during incipient faulting: The case of the Cahabón River, Guatemala, Am. J. Sci., 312, 449–507, https://doi.org/10.2475/05.2012.01, 2012.

Broccoli, A. J., Dahl, K. A., and Stouffer, R. J.: Response of the ITCZ to Northern Hemisphere cooling, Geophys. Res. Lett., 33, L01702, https://doi.org/10.1029/2005GL024546, 2006.

Brooke, S. A., Whittaker, A. C., Armitage, J. J., D'Arcy, M., and Watkins, S. E.: Quantifying sediment transport dynamics on alluvial fans from spatial and temporal changes in grain size, Death Valley, California, J. Geophys. Res.-Earth, 123, 2039–2067, https://doi.org/10.1029/2018JF004622, 2018.

Bufe, A., Burbank, D. W., Liu, L., Bookhagen, B., Qin, J., Chen, J., Li, T., Thompson Jobe, J. A., and Yang, H.: Variations of lateral bedrock erosion rates control planation of uplifting folds in the foreland of the Tian Shan, NW China, J. Geophys. Res.-Earth, 122, 2431–2467, https://doi.org/10.1002/2016JF004099, 2017.

Buter, A., Heckmann, T., Filisetti, L., Savi, S., Mao, L., Gems, B., and Comiti, F.: Effects of catchment characteristics and hydro-meteorological scenarios on sediment connectivity in glacierised catchments, Geomorphology, 402, 108128, https://doi.org/10.1016/j.geomorph.2022.108128, 2022.

Castelltort, S. and Van Den Driessche, J.: How plausible are high-frequency sediment supply-driven cycles in the stratigraphic record?, Sediment. Geol., 157, 3–13, https://doi.org/10.1016/S0037-0738(03)00066-6, 2003.

Castino, F., Bookhagen, B., and Strecker, M. R.: Rainfall variability and trends of the past six decades (1950–2014) in the subtropical NW Argentine Andes, Clim. Dynam., 48, 1049–1067, https://doi.org/10.1007/s00382-016-3127-2, 2017.

Cesta, J. M. and Ward, D. J.: Timing and nature of alluvial fan development along the Chajnantor Plateau, northern Chile, Geomorphology, 273, 412–427, https://doi.org/10.1016/j.geomorph.2016.09.003, 2016.

Clarke, L., Quine, T. A., and Nicholas, A.: An experimental investigation of autogenic behaviour during alluvial fan evolution, Geomorphology, 115, 278–285, https://doi.org/10.1016/j.geomorph.2009.06.033, 2010.

Counts, R. C., Murari, M. K., Owen, L. A., Mahan, S. A., and Greenan, M.: Late Quaternary chronostratigraphic framework of terraces and alluvium along the lower Ohio River, southwestern Indiana and western Kentucky, USA, Quaternary Sci. Rev., 110, 72–91, https://doi.org/10.1016/j.quascirev.2014.11.011, 2015.

Crivellari, S., Chiessi, C. M., Kuhnert, H., Häggi, C., da Costa Portilho-Ramos, R., Zeng, J. Y., Zhang, Y., Schefuß, E., Mollenhauer, G., Hefter, J., and Alexandre, F.: Increased Amazon freshwater discharge during late Heinrich Stadial 1, Quaternary Sci. Rev., 181, 144–155, https://doi.org/10.1016/j.quascirev.2017.12.005, 2018.

D'Arcy, M., Schildgen, T. F., Tofelde, S., Strecker, M. R., Wittmann, H., Du¨sing, W., Weissmann, P., and Roda-Boluda, D. C.: Catchment-alluvial fan systems record > 200 ka of millennial-scale climate changes in the subtropical Andes, EGU General Assembly Conference Abstracts, Vienna, 8–13 April 2018, https://ui.adsabs.harvard.edu/abs/2018EGUGA..20.4710D/abstract (last access: 4 December 2024), 2018.

D'Arcy, M. K., Schildgen, T. F., Strecker, M. R., Wittmann, H., Duesing, W., Mey, J., Tofelde, S., Weissmann, P., and Alonso, R. N.: Timing of past glaciation at the Sierra de Aconquija, northwestern Argentina, and throughout the Central Andes, Quaternary Sci. Rev., 204, 37–57, https://doi.org/10.1016/j.quascirev.2018.11.022, 2019a.

D'Arcy, M. K., Schildgen, T. F., Turowski, J. M., and Dinezio, P.: Inferring the timing of abandonment of aggraded alluvial surfaces dated with cosmogenic nuclides. Earth Surface Dynamics, 7, 755–771, https://doi.org/10.5194/esurf-7-755-2019, 2019b (code available at: https://doi.org/10.5194/esurf-7-755-2019-supplement).

DeCelles, P. G., Carrapa, B., Horton, B. K., and Gehrels, G. E.: Cenozoic foreland basin system in the central Andes of northwestern Argentina: Implications for Andean geodynamics and modes of deformation, Tectonics, 30, TC6013, https://doi.org/10.1029/2011TC002948, 2011.

Del Vecchio, J., DiBiase, R. A., Corbett, L. B., Bierman, P. R., Caffee, M. W., and Ivory, S. J.: Increased erosion rates following the onset of Pleistocene periglaciation at Bear Meadows, Pennsylvania, USA, Geophys. Res. Lett., 49, e2021GL096739, https://doi.org/10.1029/2021GL096739, 2022.

Dey, S., Thiede, R. C., Schildgen, T. F., Wittmann, H., Bookhagen, B., Scherler, D., Jain, V., and Strecker, M. R.: Climate-driven sediment aggradation and incision since the late Pleistocene in the NW Himalaya, India, Earth Planet. Sc. Lett., 449, 321–331, https://doi.org/10.1016/j.epsl.2016.05.050, 2016.

Dortch, J. M., Tomkins, M. D., Saha, S., Murari, M. K., Schoenbohm, L. M., and Curl, D.: A tool for the ages: The Probabilistic Cosmogenic Age Analysis Tool (P-CAAT), Quat. Geochronol., 71, 101323, https://doi.org/10.1016/j.quageo.2022.101323, 2022.

Dühnforth, M., Densmore, A. L., Ivy-Ochs, S., Allen, P. A., and Kubik, P. W.: Timing and patterns of debris flow deposition on Shepherd and Symmes creek fans, Owens Valley, California, deduced from cosmogenic ^{10}Be, J. Geophys. Res.-Earth, 112, F03S15, https://doi.org/10.1029/2006JF000562, 2007.

Dühnforth, M., Densmore, A. L., Ivy-Ochs, S., Allen, P., and Kubik, P. W.: Early to Late Pleistocene history of debris-flow fan evolution in western Death Valley (California) using cosmogenic ^{10}Be and ^{26}Al, Geomorphology, 281, 53–65, https://doi.org/10.1016/j.geomorph.2016.12.020, 2017.

Dunai, T. J., Loìpez, G. A. G., and Juez-Larré, J.: Oligocene–Miocene age of aridity in the Atacama Desert revealed by exposure dating of erosion-sensitive landforms, Geology, 33, 321–324, https://doi.org/10.1130/G21184.1, 2005.

Fisher, G. B., Luna, L. V., Amidon, W. H., Burbank, D. W., de Boer, B., Stap, L. B., Bookhagen, B., Godard, V., Oskin, M. E., Alonso, R. N., and Tuenter, E.: Milankovitch-paced erosion in the southern Central Andes, Nat. Commun., 14, 424, https://doi.org/10.1038/s41467-023-36022-0, 2023.

Fritz, S. C., Baker, P. A., Lowenstein, T. K., Seltzer, G. O., Rigsby, C. A., Dwyer, G. S., Tapia, P. M., Arnold, K. K., Ku, T. L., and Luo, S.: Hydrologic variation during the last 170,000 years in the southern hemisphere tropics of South America, Quaternary Res., 61, 95–104, https://doi.org/10.1016/j.yqres.2003.08.007, 2004.

Fritz, S. C., Baker, P. A., Seltzer, G. O., Ballantyne, A., Tapia, P., Cheng, H., and Edwards, R. L.: Quaternary glaciation and hydrologic variation in the South American tropics as reconstructed from the Lake Titicaca drilling project, Quaternary Res., 68, 410–420, https://doi.org/10.1016/j.yqres.2007.07.008, 2007.

Fritz, S. C., Baker, P. A., Ekdahl, E., Seltzer, G. O., and Stevens, L. R.: Millennial-scale climate variability during the Last Glacial period in the tropical Andes, Quaternary Sci. Rev., 29, 1017–1024, https://doi.org/10.1016/j.quascirev.2010.01.001, 2010.

Fryirs, K. A., Brierley, G. J., Preston, N. J., and Kasai, M.: Buffers, barriers and blankets: The (dis) connectivity of catchment-scale sediment cascades, Catena, 70, 49–67, https://doi.org/10.1016/j.catena.2006.07.007, 2007.

Ganev, P. N., Dolan, J. F., Frankel, K. L., and Finkel, R. C.: Rates of extension along the Fish Lake Valley fault and transtensional deformation in the Eastern California shear zone–Walker Lane belt, Lithosphere, 2, 33–49, https://doi.org/10.1130/L51.1, 2010.

García, V. H., Hongn, F., and Cristallini, E. O.: Late Miocene to recent morphotectonic evolution and potential seismic hazard of the northern Lerma valley: clues from Lomas de Medeiros, Cordillera Oriental, NW Argentina, Tectonophysics, 608, 1238–1253, https://doi.org/10.1016/j.tecto.2013.06.021, 2013.

Godard, V., Tucker, G. E., Burch Fisher, G., Burbank, D. W., and Bookhagen, B.: Frequency-dependent landscape response to climatic forcing, Geophys. Res. Lett., 40, 859–863, https://doi.org/10.1002/grl.50253, 2013.

Godfrey, L. V., Jordan, T. E., Lowenstein, T. K., and Alonso, R. L.: Stable isotope constraints on the transport of water to the Andes between 22 and 26 S during the last glacial cycle, Palaeogeogr. Palaeocl., 194, 299–317, https://doi.org/10.1016/S0031-0182(03)00283-9, 2003.

Gosling, W. D., Bush, M. B., Hanselman, J. A., and Chepstow-Lusty, A.: Glacial-interglacial changes in moisture balance and the impact on vegetation in the southern hemisphere tropical Andes (Bolivia/Peru), Palaeogeogr. Palaeocl., 259, 35–50, https://doi.org/10.1016/j.palaeo.2007.02.050, 2008.

Gray, H. J., Owen, L. A., Dietsch, C., Beck, R. A., Caffee, M. A., Finkel, R. C., and Mahan, S. A.: Quaternary landscape development, alluvial fan chronology and erosion of the Mecca Hills at the southern end of the San Andreas fault zone, Quaternary Sci. Rev., 105, 66–85, https://doi.org/10.1016/j.quascirev.2014.09.009, 2014.

Guarnieri, P. and Pirrotta, C.: The response of drainage basins to the late Quaternary tectonics in the Sicilian side of the Messina Strait (NE Sicily), Geomorphology, 95, 260–273, https://doi.org/10.1016/j.geomorph.2007.06.013, 2008.

Gulick, S. P., Jaeger, J. M., Mix, A. C., Asahi, H., Bahlburg, H., Belanger, C. L., Berbel, G. B., Childress, L., Cowan, E., Drab, L., and Forwick, M.: Mid-Pleistocene climate transition drives net mass loss from rapidly uplifting St. Elias Mountains, Alaska, P. Natl. Acad. Sci. USA, 112, 15042–15047, https://doi.org/10.1073/pnas.1512549112, 2015.

Haeuselmann, P., Granger, D. E., Jeannin, P. Y., and Lauritzen, S. E.: Abrupt glacial valley incision at 0.8 Ma dated from cave deposits in Switzerland, Geology, 35, 143–146, https://doi.org/10.1130/G23094A, 2007.

Hain, M. P., Strecker, M. R., Bookhagen, B., Alonso, R. N., Pingel, H., and Schmitt, A. K.: Neogene to Quaternary broken foreland formation and sedimentation dynamics in the Andes of NW Argentina (25° S), Tectonics, 30, TC2006, https://doi.org/10.1029/2010TC002703, 2011.

Harvey, A. M.: The coupling status of alluvial fans and debris cones: a review and synthesis, Earth Surf. Proc. Land., 37, 64–76, https://doi.org/10.1002/esp.2213, 2012.

Harvey, A. M., Silva, P. G., Mather, A. E., Goy, J. L., Stokes, M., and Zazo, C.: The impact of Quaternary sea-level and climatic change on coastal alluvial fans in the Cabo

de Gata ranges, southeast Spain, Geomorphology, 28, 1–22, https://doi.org/10.1016/S0169-555X(98)00100-7, 1999.

Haselton, K., Hilley, G., and Strecker, M. R.: Average Pleistocene climatic patterns in the southern central Andes: Controls on mountain glaciation and paleoclimate implications, J. Geol., 110, 211–226. 2002.

Hedrick, K., Owen, L. A., Rockwell, T. K., Meigs, A., Costa, C., Caffee, M. W., Masana, E., and Ahumada, E.: Timing and nature of alluvial fan and strath terrace formation in the Eastern Precordillera of Argentina, Quaternary Sci. Rev., 80, 143–168, https://doi.org/10.1016/j.quascirev.2013.05.004, 2013.

Hidy, A. J., Gosse, J. C., Pederson, J. L., Mattern, J. P., and Finkel, R. C.: A geologically constrained Monte Carlo approach to modeling exposure ages from profiles of cosmogenic nuclides: An example from Lees Ferry, Arizona, Geochem. Geophy. Geosy., 11, Q0AA10, https://doi.org/10.1029/2010GC003084, 2010.

Hilley, G. E. and Strecker, M. R.: Processes of oscillatory basin filling and excavation in a tectonically active orogen: Quebrada del Toro Basin, NW Argentina, Bull. Geol. Soc. Am., 117, 887–901, https://doi.org/10.1130/B25602.1, 2005.

Howard, A. D.: Equilibrium and time scales in geomorphology: Application to sand-bed alluvial streams, Earth Surf. Proc. Land., 7, 303–325, https://doi.org/10.1002/esp.3290070403, 1982.

Hughes, P. D.: Geomorphology and Quaternary stratigraphy: The roles of morpho-, litho-, and allostratigraphy, Geomorphology, 123, 189–199, https://doi.org/10.1016/j.geomorph.2010.07.025, 2010.

Imbrie, J. D. and McIntyre, A.: SST vs time for core RC24-16 (specmap.056), PANGAEA [data set], https://doi.org/10.1594/PANGAEA.441754, 2006.

Kelly, M. A., Lowell, T. V., Applegate, P. J., Phillips, F. M., Schaefer, J. M., Smith, C. A., Kim, H., Leonard, K. C., and Hudson, A. M.: A locally calibrated, late glacial ^{10}Be production rate from a low-latitude, high-altitude site in the Peruvian Andes, Quat. Geochronol., 26, 70–85, https://doi.org/10.1016/j.quageo.2013.10.007, 2015.

Kleinert, K. and Strecker, M. R.: Climate change in response to orographic barrier uplift: Paleosol and stable isotope evidence from the late Neogene Santa Maria basin, northwestern Argentina, Geol. Soc. Am. Bull., 113, 728–742, https://doi.org/10.1130/0016-7606(2001)113<0728:CCIRTO>2.0.CO;2, 2001.

Kober, F., Zeilinger, G., Ivy-Ochs, S., Dolati, A., Smit, J., and Kubik, P. W.: Climatic and tectonic control on fluvial and alluvial fan sequence formation in the Central Makran Range, SE-Iran, Global Planet. Change, 111, 133–149, https://doi.org/10.1016/j.gloplacha.2013.09.003, 2013.

Lifton, N., Sato, T., and Dunai, T. J.: Scaling in situ cosmogenic nuclide production rates using analytical approximations to atmospheric cosmic-ray fluxes, Earth Planet. Sc. Lett., 386, 149–160, https://doi.org/10.1016/j.epsl.2013.10.052, 2014.

Lisiecki, L. E. and Raymo, M. E.: Diachronous benthic δ^{18}O responses during late Pleistocene terminations, Paleoceanography, 24, PA3210, https://doi.org/10.1029/2009PA001732, 2009.

Luna, L. V., Bookhagen, B., Niedermann, S., Rugel, G., Scharf, A., and Merchel, S.: Glacial chronology and production rate cross-calibration of five cosmogenic nuclide and mineral systems from the southern Central Andean Plateau, Earth Planet. Sc. Lett., 500, 242–253, https://doi.org/10.1016/j.epsl.2018.07.034, 2018.

Ma, Y. and Stuart, F. M.: The use of in-situ cosmogenic ^{21}Ne in studies on long-term landscape development, Acta Geochimica, 37, 310–322, https://doi.org/10.1007/s11631-017-0216-9, 2018.

Mackin, J.: Concept of the graded river, Geol. Soc. Am. Bull., 59, 463–512, 1948.

Malamud, B. D., Jordan, T. E., Alonso, R. A., Gallardo, E. F., Gonzalez, R. E., and Kelley, S. A.: Pleistocene Lake Lerma, Salta Province, NW Argentina, in: XIII Congreso Geológico Argentino y III Congreso de Exploración de Hidrocarburos, Buenos Aires, 13–18 October 1996, Vol. 1, 103–114, 1996.

Marrett, R. and Strecker, M. R.: Response of intracontinental deformation in the central Andes to late Cenozoic reorganization of South American Plate motions, Tectonics, 19, 452–467, https://doi.org/10.1029/1999TC001102, 2000.

Marrett, R. A., Allmendinger, R. W., Alonso, R. N., and Drake, R. E.: Late Cenozoic tectonic evolution of the Puna Plateau and adjacent foreland, northwestern Argentine Andes, J. S. Am. Earth Sci., 7, 179–207, https://doi.org/10.1016/0895-9811(94)90007-8, 1994.

Martin, L. C., Blard, P. H., Lavé, J., Condom, T., Prémaillon, M., Jomelli, V., Brunstein, D., Lupker, M., Charreau, J., Mariotti, V., and Tibari, B.: Lake Tauca highstand (Heinrich Stadial 1a) driven by a southward shift of the Bolivian High, Science Advances, 4, https://doi.org/10.1126/sciadv.aar2514, 2018.

Martin, L. C. P., Blard, P.-H., Lavé, J., Braucher, R., Lupker, M., Condom, T., Charreau, J., Mariotti, V., ASTER Team, and Davy, E.: In situ cosmogenic ^{10}Be production rate in the High Tropical Andes, Quat. Geochronol., 30, 54–68, https://doi.org/10.1016/j.quageo.2015.06.012, 2015.

Martin, L. C. P., Blard, P.-H., Balco, G., Lavé, J., Delunel, R., Lifton, N., and Laurent, V.: The CREp program and the ICE-D production rate calibration database: A fully parameterizable and updated online tool to compute cosmic-ray exposure ages, Quat. Geochronol., 38, 25–49, https://doi.org/10.1016/j.quageo.2016.11.006, 2017.

Martini, M. A., Kaplan, M. R., Strelin, J. A., Astini, R. A., Schaefer, J. M., Caffee, M. W., and Schwartz, R.: Late Pleistocene glacial fluctuations in Cordillera oriental, subtropical Andes, Quaternary Sci. Rev., 171, 245–259, https://doi.org/10.1016/j.quascirev.2017.06.033, 2017.

Mather, A. E., Stokes, M., and Whitfield, E.: River terraces and alluvial fans: The case for an integrated Quaternary fluvial archive, Quaternary Sci. Rev., 166, 74–90, https://doi.org/10.1016/j.quascirev.2016.09.022, 2017.

Mazzuoli, R., Vezzoli, L., Omarini, R., Acocella, V., Gioncada, A., Matteini, M., Dini, A., Guillou, H., Hauser, N., Uttini, A., and Scaillet, S.: Miocene magmatism and tectonics of the easternmost sector of the Calama–Olacapato–El Toro fault system in Central Andes at ∼ 24° S: Insights into the evolution of the Eastern Cordillera, GSA Bulletin, 120, 1493–1517, https://doi.org/10.1130/B26109.1, 2008.

McFadden, L. D., Ritter, J. B., and Wells, S. G.: Use of Multi-parameter Relative-Age Methods for Age Estimation and Correlation of Alluvial Fan Surfaces on a Desert Piedmont, Eastern Mojave Desert, California, Quaternary Res., 32, 276–290, https://doi.org/10.1016/0033-5894(89)90094-X, 1989.

McIntyre, A. and Imbrie, J. D.: Stable isotopes of sediment core V30-40 (specmap.010), PANGAEA [data set], https://doi.org/10.1594/PANGAEA.56361, 2000.

McNab, F., Schildgen, T. F., Turowski, J. M., and Wickert, A. D.: Diverse responses of alluvial rivers to periodic environmental change, Geophys. Res. Lett., 50, e2023GL103075, https://doi.org/10.1029/2023GL103075, 2023.

Mescolotti, P. C., do Nascimento Pupim, F., Ladeira, F. S. B., Sawakuchi, A. O., Santa Catharina, A., and Assine, M. L.: Fluvial aggradation and incision in the Brazilian tropical semi-arid: Climate-controlled landscape evolution of the São Francisco River, Quaternary Sci. Rev., 263, 106977, https://doi.org/10.1016/j.quascirev.2021.106977, 2021.

Mey, J., D'Arcy, M. K., Schildgen, T. F., Egholm, D. L., Wittmann, H., and Strecker, M. R.: Temperature and precipitation in the southern Central Andes during the last glacial maximum, Heinrich Stadial 1, and the Younger Dryas, Quaternary Sci. Rev., 248, 106592, https://doi.org/10.1016/j.quascirev.2020.106592, 2020.

Milanez Fernandes, V., Schildgen, T., Ruby, A., Wittmann-Oelze, H., and McNab, F.: Pleistocene Landscape Evolution in Southern Patagonia: A Record of Regional Incision from ^{10}Be Dating of Fluvial Terraces, EGU General Assembly 2023, Vienna, Austria, 23–28 Apr 2023, EGU23-15938, https://doi.org/10.5194/egusphere-egu23-15938, 2023.

Mosblech, N. A., Bush, M. B., Gosling, W. D., Hodell, D., Thomas, L., Van Calsteren, P., Correa-Metrio, A., Valencia, B. G., Curtis, J., and Van Woesik, R.: North Atlantic forcing of Amazonian precipitation during the last ice age, Nat. Geosci., 5, 817–820, https://doi.org/10.1038/ngeo1588, 2012.

Mouchené, M., van der Beek, P., Carretier, S., and Mouthereau, F.: Autogenic versus allogenic controls on the evolution of a coupled fluvial megafan–mountainous catchment system: numerical modelling and comparison with the Lannemezan megafan system (northern Pyrenees, France), Earth Surf. Dynam., 5, 125–143, https://doi.org/10.5194/esurf-5-125-2017, 2017.

Mouslopoulou, V., Begg, J., Fülling, A., Moraetis, D., Partsinevelos, P., and Oncken, O.: Distinct phases of eustatic and tectonic forcing for late Quaternary landscape evolution in southwest Crete, Greece, Earth Surf. Dynam., 5, 511–527, https://doi.org/10.5194/esurf-5-511-2017, 2017.

Nicholas, A. P. and Quine, T. A.: Modeling alluvial landform change in the absence of external environmental forcing, Geology, 35, 527–530, https://doi.org/10.1130/G23377A.1, 2007.

Novello, V. F., Cruz, F. W., Vuille, M., Stríkis, N. M., Edwards, R. L., Cheng, H., Emerick, S., De Paula, M. S., Li, X., Barreto, E. D. S., and Karmann, I.: A high-resolution history of the South American Monsoon from Last Glacial Maximum to the Holocene, Sci. Rep., 7, 44267, https://doi.org/10.1038/srep44267, 2017.

Orr, E. N., Owen, L. A., Saha, S., and Caffee, M. W.: Climate-driven late Quaternary fan surface abandonment in the NW Himalaya, in: Untangling the Quaternary Period—A Legacy of Stephen C. Porter, edited by: Waitt, R. B., Thackray, G. D., and Gillespie, A. R., Geological Society of America, 63–80, https://doi.org/10.1130/2020.2548(04), 2021.

Owen, L. A., Clemmens, S. J., Finkel, R. C., and Gray, H.: Late Quaternary alluvial fans at the eastern end of the San Bernardino Mountains, Southern California, Quaternary Sci. Rev., 87, 114–134, https://doi.org/10.1016/j.quascirev.2014.01.003, 2014.

Paola, C., Heller, P. L., and Angevine, C. L.: The large-scale dynamics of grain-size variation in alluvial basins, 1: theory, Basin Res., 4, 73–90, https://doi.org/10.1111/j.1365-2117.1992.tb00145.x, 1992.

Pearson, D. M., Kapp, P., DeCelles, P. G., Reiners, P. W., Gehrels, G. E., Ducea, M. N., and Pullen, A.: Influence of pre-Andean crustal structure on Cenozoic thrust belt kinematics and shortening magnitude: Northwestern Argentina, Geosphere, 9, 1766–1782, 2013, https://doi.org/10.1130/GES00923.1.

Pedersen, V. K. and Egholm, D. L.: Glaciations in response to climate variations preconditioned by evolving topography, Nature, 493, 206–210, https://doi.org/10.1038/nature11786, 2013.

Peri, V. G., Haghipour, N., Christl, M., Terrizzano, C., Kaveh-Firouz, A., Leiva, M. F., Pérez, P., Yamin, M., Barcelona, H., and Burg, J. P.: Quaternary landscape evolution in the Western Argentine Precordillera constrained by ^{10}Be cosmogenic dating, Geomorphology, 396, 107984, https://doi.org/10.1016/j.geomorph.2021.107984, 2022.

Pingel, H., Strecker, M. R., Alonso, R. N., and Schmitt, A. K.: Neotectonic basin and landscape evolution in the Eastern Cordillera of NW Argentina, Humahuaca Basin (∼ 24 S), Basin Res., 25, 554–573, https://doi.org/10.1111/bre.12016, 2013.

Pingel, H., Mulch, A., Alonso, R. N., Cottle, J., Hynek, S. A., Poletti, J., Rohrmann, A., Schmitt, A. K., Stockli, D. F., and Strecker, M. R.: Surface uplift and convective rainfall along the southern Central Andes (Angastaco Basin, NW Argentina), Earth Planet. Sc. Lett., 440, 33–42, https://doi.org/10.1016/j.epsl.2016.02.009, 2016.

Pingel, H., Alonso, R. N., Altenberger, U., Cottle, J., and Strecker, M. R.: Miocene to Quaternary basin evolution at the southeastern Andean Plateau (Puna) margin (ca. 24° S lat, Northwestern Argentina), Basin Res., 31, 808–826, https://doi.org/10.1111/bre.12346, 2019a.

Pingel, H., Schildgen, T., Strecker, M. R., and Wittmann, H.: Pliocene–Pleistocene orographic control on denudation in northwest Argentina, Geology, 47, 359–362, https://doi.org/10.1130/G45800.1, 2019b.

Pingel, H., Strecker, M. R., Mulch, A., Alonso, R. N., Cottle, J., and Rohrmann, A.: Late Cenozoic topographic evolution of the Eastern Cordillera and Puna Plateau margin in the southern Central Andes (NW Argentina), Earth Planet. Sc. Lett., 535, 116112, https://doi.org/10.1016/j.epsl.2020.116112, 2020.

Phillips, F. M., Zreda, M. G., Smith, S. S., Elmore, D., Kubik, P. W., and Sharma, P.: Cosmogenic chlorine-36 chronology for glacial deposits at Bloody Canyon, eastern Sierra Nevada, Science, 248, 1529–1532, https://doi.org/10.1126/science.248.4962.1529, 1990.

Placzek, C., Quade, J., and Patchett, P. J.: Geochronology and stratigraphy of late Pleistocene lake cycles on the southern Bolivian Altiplano: implications for causes of tropical climate change, Geol. Soc. Am. Bull., 118, 515–532, https://doi.org/10.1130/B25770.1, 2006.

Prush, V. B. and Oskin, M. E.: A mechanistic erosion model for cosmogenic nuclide inheritance in single-clast exposure ages, Earth Planet. Sc. Lett., 535, 116066, https://doi.org/10.1016/j.epsl.2020.116066, 2020.

Ratnayaka, K., Hetzel, R., Hornung, J., Hampel, A., Hinderer, M., and Frechen, M.: Postglacial alluvial fan dynamics in the Cordillera Oriental, Peru, and palaeoclimatic implications, Quaternary Res., 91, 431–449, https://doi.org/10.1017/qua.2018.106, 2019.

Robinson, R. A. J., Spencer, J. Q. G., Strecker, M. R., Richter, A., and Alonso, R. N.: Luminescence dating of alluvial fans in intramontane basins of NW Argentina, in: Alluvial Fans: Geomorphology, Sedimentology, Dynamics, edited by: Harvey, A. M., Mather, A. E., and Stokes, M., Geol. Soc. Sp., 251, 153–168. 2005.

Rohais, S., Bonnet, S., and Eschard, R.: Sedimentary record of tectonic and climatic erosional perturbations in an experimental coupled catchment-fan system, Basin Res., 24, 198–212, https://doi.org/10.1111/j.1365-2117.2011.00520.x, 2012.

Romans, B. W., Castelltort, S., Covault, J. A., Fildani, A., and Walsh, J. P.: Environmental signal propagation in sedimentary systems across timescales, Earth-Sci. Rev., 153, 7–29, https://doi.org/10.1016/j.earscirev.2015.07.012, 2016.

Savi, S., Schildgen, T. F., Tofelde, S., Wittmann, H., Scherler, D., Mey, J., Alonso, R. N., and Strecker, M. R.: Climatic controls on debris-flow activity and sediment aggradation: The Del Medio fan, NW Argentina, J. Geophys. Res.-Earth, 121, 2424–2445, https://doi.org/10.1002/2016JF003912, 2016.

Savi, S., Tofelde, S., Wickert, A. D., Bufe, A., Schildgen, T. F., and Strecker, M. R.: Interactions between main channels and tributary alluvial fans: channel adjustments and sediment-signal propagation, Earth Surf. Dynam., 8, 303–322, https://doi.org/10.5194/esurf-8-303-2020, 2020.

Schildgen, T. F., Robinson, R. A. J., Savi, S., Phillips, W. M., Spencer, J. Q. G., Bookhagen, B., Scherler, D., Tofelde, S., Alonso, R. N., Kubik, P. W., Binnie, S. A., and Strecker, M. R.: Landscape response to late Pleistocene climate change in NW Argentina: Sediment flux modulated by basin geometry and connectivity, J. Geophys. Res.-Earth 121, 392–414, https://doi.org/10.1002/2015JF003607, 2016.

Schwab, K. and Schäfer, A.: Sedimentation und Tektonik im mittleren Abschnitt des Río Toro in der Ostkordillere NW-Argentiniens, Geol. Rundsch., 65, 175–194, https://doi.org/10.1007/BF01808462, 1976.

Schwanghart, W. and Scherler, D.: Short Communication: Topo-Toolbox 2 – MATLAB-based software for topographic analysis and modeling in Earth surface sciences, Earth Surf. Dynam., 2, 1–7, https://doi.org/10.5194/esurf-2-1-2014, 2014.

Simpson, G. and Castelltort, S.: Model shows that rivers transmit high-frequency climate cycles to the sedimentary record, Geology, 40, 1131–1134, https://doi.org/10.1130/G33451.1, 2012.

Seagren, E. G. and Schoenbohm, L. M.: Drainage reorganization across the Puna Plateau margin (NW Argentina): Implications for the preservation of orogenic plateaus, J. Geophys. Res.-Earth, 126, e2021JF006147, https://doi.org/10.1029/2021JF006147, 2021.

Seagren, E. G., McMillan, M., and Schoenbohm, L. M.: Tectonic control on drainage evolution in broken forelands: Examples from NW Argentina, Tectonics, 41, e2020TC006536, https://doi.org/10.1029/2020TC006536, 2022.

Spelz, R. M., Fletcher, J. M., Owen, L. A., and Caffee, M. W.: Quaternary alluvial-fan development, climate and morphologic dating of fault scarps in Laguna Salada, Baja California, Mexico, Geomorphology, 102, 578–594, https://doi.org/10.1016/j.geomorph.2008.06.001, 2008.

Steffen, D., Schlunegger, F., and Preusser, F.: Drainage basin response to climate change in the Pisco valley, Peru. Geology, 37, 491–494, https://doi.org/10.1130/G25475A.1, 2009.

Steffen, D., Schlunegger, F., and Preusser, F.: Late Pleistocene fans and terraces in the Majes valley, southern Peru, and their relation to climatic variations, Int. J. Earth Sci., 99, 1975–1989, https://doi.org/10.1007/s00531-009-0489-2, 2010.

Sternai, P., Herman, F., Valla, P. G., and Champagnac, J. D.: Spatial and temporal variations of glacial erosion in the Rhône valley (Swiss Alps): Insights from numerical modeling, Earth Planet. Sc. Lett., 368, 119–131, https://doi.org/10.1016/j.epsl.2013.02.039, 2013.

Strecker, M. R., Alonso, R. N., Bookhagen, B., Carrapa, B., Hilley, G. E., Sobel, E. R., and Trauth, M. H.: Tectonics and climate of the southern central Andes, Annu. Rev. Earth Pl. Sc., 35, 747–787, https://doi.org/10.1146/annurev.earth.35.031306.140158, 2007.

Strecker, M. R., Alonso, R., Bookhagen, B., Carrapa, B., Coutand, I., Hain, M. P., Hilley, G. E., Mortimer, E., Schoenbohm, L., and Sobel, E. R.: Does the topographic distribution of the central Andean Puna Plateau result from climatic or geodynamic processes?, Geology, 37, 643–646, https://doi.org/10.1130/G25545A.1, 2009.

Streit, R. L., Burbank, D. W., Strecker, M. R., Alonso, R. N., Cottle, J. M., and Kylander-Clark, A. R. C.: Controls on intermontane basin filling, isolation and incision on the margin of the Puna Plateau, NW Argentina ($\sim 23°$ S), Basin Res., 29, 131–155, https://doi.org/10.1111/bre.12141, 2017.

Terrizzano, C. M., García Morabito, E., Christl, M., Likerman, J., Tobal, J., Yamin, M., and Zech, R.: Climatic and Tectonic forcing on alluvial fans in the Southern Central Andes, Quaternary Sci. Rev., 172, 131–141, https://doi.org/10.1016/j.quascirev.2017.08.002, 2017.

Tobal, J. E., Morabito, E. G., Terrizzano, C. M., Zech, R., Colavitto, B., Struck, J., Christl, M., and Ghiglione, M. C.: Quaternary landscape evolution of Patagonia at the Chilean Triple Junction: Climate and tectonic forcings, Quaternary Sci. Rev., 261, 106960, https://doi.org/10.1016/j.quascirev.2021.106960, 2021.

Tofelde, S., Schildgen, T. F., Savi, S., Pingel, H., Wickert, A. D., Bookhagen, B., Wittmann, H., Alonso, R. N., Cottle, J., and Strecker, M. R.: 100 kyr fluvial cut-and-fill terrace cycles since the Middle Pleistocene in the southern Central Andes, NW Argentina, Earth Planet. Sc. Lett., 473, 141–153, https://doi.org/10.1016/j.epsl.2017.06.001, 2017.

Tofelde, S., Duesing, W., Schildgen, T. F., Wickert, A. D., Wittmann, H., Alonso, R. N., and Strecker, M.: Effects of deep-seated versus shallow hillslope processes on cosmogenic [10]Be concentrations in fluvial sand and gravel, Earth Surf. Proc. Landf., 43, 3086–3098, https://doi.org/10.1002/esp.4471, 2018.

Tofelde, S., Savi, S., Wickert, A. D., Bufe, A., and Schildgen, T. F.: Alluvial channel response to environmental perturbations: fill-terrace formation and sediment-signal disruption, Earth Surf. Dynam., 7, 609–631, https://doi.org/10.5194/esurf-7-609-2019, 2019.

Tofelde, S., Bernhardt, A., Guerit, L., and Romans, B. W.: Times associated with source-to-sink propagation of environmental signals during landscape transience, Front. Earth Sci., 9, 628315, https://doi.org/10.3389/feart.2021.628315, 2021.

Uppala, S. M., Kållberg, P. W., Simmons, A. J., Andrae, U., Bechtold, V. D. C., Fiorino, M., Gibson, J. K., Haseler, J., Hernandez, A., Kelly, G. A., Li, X., Onogi, K., Saarinen, S., Sokka, N., Allan, R. P., Andersson, E., Arpe, K., Balmaseda, M. A., Beljaars,

A. C. M., Berg, L. Van De, Bidlot, J., Bormann, N., Caires, S., Chevallier, F., Dethof, A., Dragosavac, M., Fisher, M., Fuentes, M., Hagemann, S., Hólm, E., Hoskins, B. J., Isaksen, L., Janssen, P. A. E. M., Jenne, R., Mcnally, A. P., Mahfouf, J.-F., Morcrette, J.-J., Rayner, N. A., Saunders, R. W., Simon, P., Sterl, A., Trenberth, K. E., Untch, A., Vasiljevic, D., Viterbo, P., and Woollen, J.: The ERA-40 re-analysis, Q. J. Roy. Meteor. Soc., 131, 2961–3012, https://doi.org/10.1256/qj.04.176, 2005.

Valla, P. G., Shuster, D. L., and Van Der Beek, P. A.: Significant increase in relief of the European Alps during mid-Pleistocene glaciations, Nat. Geosci., 4, 688–692, https://doi.org/10.1038/ngeo1242, 2011.

van den Berg, A. P. H., van Saparoea, V., and Postma, G.: Control of climate change on the yield of river systems, in: Recent Advances in Models of Siliciclastic Shallow-Marine Stratigraphy, edited by: Hampson, G. J., Steel, R. J., Burgess, P. M., and Dalrymple, R. W., SEPM Spec. P., 90, 15–33, https://doi.org/10.2110/pec.08.90.0015, 2008.

Ventra, D. and Nichols, G. J.: Autogenic dynamics of alluvial fans in endorheic basins: outcrop examples and stratigraphic significance, Sedimentology, 61, 767–791, https://doi.org/10.1111/sed.12077, 2014.

Vera, C., Higgins, W., Amador, J., Ambrizzi, T., Garreaud, R., Gochis, D., Gutzler, D., Lettenmaier, D., Marengo, J., Mechoso, C. R., and Nogues-Paegle, J.: Toward a unified view of the American monsoon systems, J. Climate, 19, 4977–5000, https://doi.org/10.1175/JCLI3896.1, 2006.

Vezzoli, L., Acocella, V., Omarini, R., and Mazzuoli, R.: Miocene sedimentation, volcanism and deformation in the Eastern Cordillera (24°30′ S, NW Argentina): Tracking the evolution of the foreland basin of the Central Andes, Basin Res., 24, 637–663, https://doi.org/10.1111/j.1365-2117.2012.00547.x, 2012.

Vizy, E. K. and Cook, K. H.: Relationship between Amazon and high Andes rainfall, J. Geophys. Res.-Atmos., 112, D07107, https://doi.org/10.1029/2006JD007980, 2007.

von Blanckenburg, F., Hewawasam, T., and Kubik, P.: Cosmogenic nuclide evidence for low weathering and denudation in the wet, tropical highlands of Sri Lanka, J. Geophys. Res.-Earth, 109, https://doi.org/10.1029/2003jf000049, 2004.

Wang, X., Auler, A. S., Edwards, R. L., Cheng, H., Ito, E., Wang, Y., Kong, X., and Solheid, M.: Millennial-scale precipitation changes in southern Brazil over the past 90,000 years, Geophys. Res. Lett., 34, L23701, https://doi.org/10.1029/2007GL031149, 2007.

Wickert, A. D. and Schildgen, T. F.: Long-profile evolution of transport-limited gravel-bed rivers, Earth Surf. Dynam., 7, 17–43, https://doi.org/10.5194/esurf-7-17-2019, 2019.

Wittmann, H., Malusà, M. G., Resentini, A., Garzanti, E., and Niedermann, S.: The cosmogenic record of mountain erosion transmitted across a foreland basin: Source-to-sink analysis of in situ ^{10}Be, ^{26}Al and ^{21}Ne in sediment of the Po river catchment, Earth Planet. Sc. Lett., 452, 258–271, https://doi.org/10.1016/j.epsl.2016.07.017, 2016.

Zech, J., Terrizzano, C. M., Garcia Morabito, E., Veit, H., and Zech, R.: Timing and extent of late Pleistocene glaciation in the arid Central Andes of Argentina and Chile (22°–41° S), CIG, 43, 697–718, https://doi.org/10.18172/cig.3235, 2017.

Zondervan, J. R., Stokes, M., Boulton, S. J., Telfer, M. W., and Mather, A. E.: Rock strength and structural controls on fluvial erodibility: Implications for drainage divide mobility in a collisional mountain belt, Earth Planet. Sc. Lett., 538, 116221, https://doi.org/10.1016/j.epsl.2020.116221, 2020.